Journal of Sustainable Metallurgy (2026) 12:971–993
https://doi.org/10.1007/s40831-025-01371-1

REVIEW ARTICLE

Trends and Challenges in Lead-Free Brass Alloy Development for Machining Applications: A Systematic Literature Review

Bernardo L. Ribeiro[1,2] · José Monteiro[1,2] · Mariana Truta[1,2] · Rúben F. Santos[1,2] · Maria Barbosa[3] · Elsa W. Sequeiros[1,2]

Received: 8 September 2025 / Accepted: 2 December 2025 / Published online: 14 January 2026

Abstract
Lead (Pb) is widely used in brass alloys (Cu–Zn) to enhance machinability, as its deformation into needle-like particles promotes chip breakage by initiating cracks. However, growing awareness of Pb's toxicity has led to strict environmental regulations and growing demand for sustainable, lead-free alternatives. This systematic review, conducted following the PRISMA 2020 framework, consolidates recent research on the development and performance of machinable lead-free brass alloys. A comprehensive search was performed in the Web of Science, ScienceDirect, and Scopus databases, identifying 93 studies for full-text analysis. Various strategies have been identified for the development of lead-free brass, including process optimization, heat treatments, direct Pb substitution, and novel alloy design. The review highlights significant progress in achieving acceptable mechanical and machining performance, although trade-offs in cost, corrosion resistance, and large-scale manufacturability remain. The consolidated key findings offer a structured basis for future alloy design and promote consistent evaluation of microstructural, mechanical, and machining properties.

The contributing editor for this article was U. Pal.

✉ Bernardo L. Ribeiro
up201806499@fe.up.pt

[1] DEMec – Faculdade de Engenharia, Universidade Do Porto, Rua Dr. Roberto Frias, 4200-465 Porto, Portugal

[2] LAETA - Institute of Science and Innovation in Mechanical and Industrial Engineering, 4200-465 Porto, Portugal

[3] ASBW - Barbosa World Brass S.A., 4525-100 Canedo VFR, Portugal

Graphical Abstract

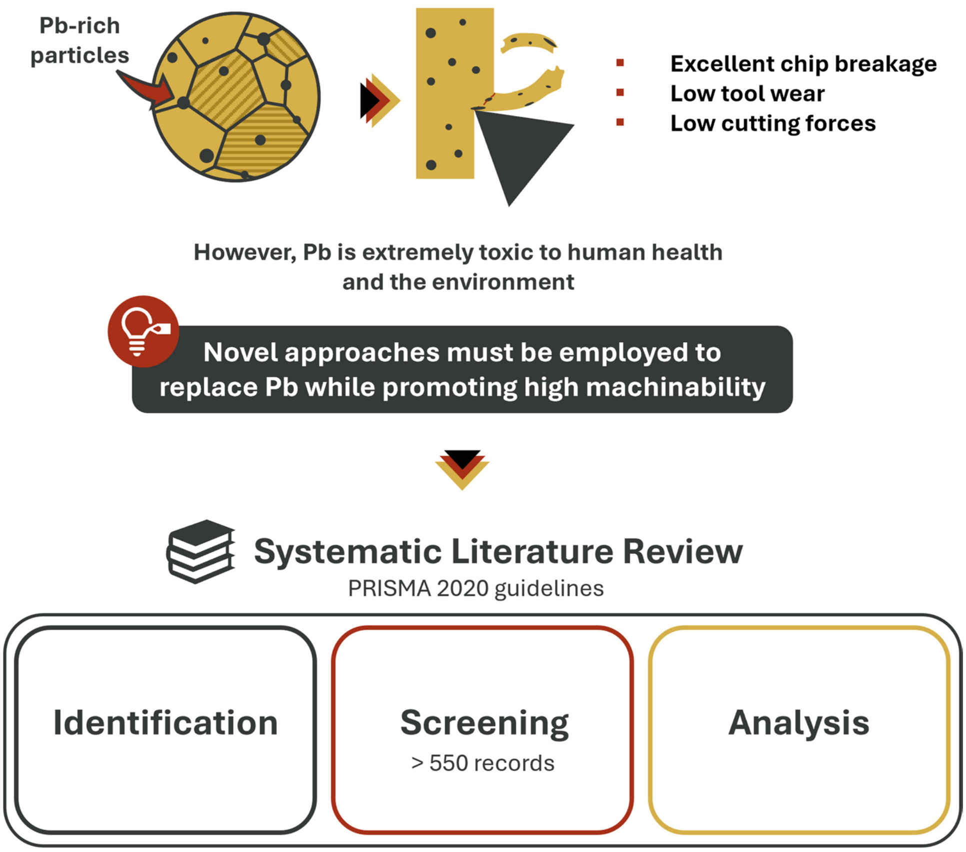

Keywords Alloy design · Brass · Heat treatment · Lead-free · Machining · Optimization

Introduction

Copper–zinc (Cu–Zn)-based alloys, also known as brass alloys, are among the most widely used engineering materials due to their corrosion resistance, low friction coefficient, forgeability, and machinability [1]. The Cu/Zn ratio can highly influence the properties of such alloys. However, due to the increasing industrial demands, other elements are usually added to improve the alloys' overall performance [2, 3]. Lead (Pb) has been commonly added to brass alloys (~2–4 wt%) to aid in subtractive manufacturing, as it enhances fundamental processing properties, such as machinability. Pb is virtually insoluble in the Cu–Zn system, leading to the formation of spherical Pb-rich inclusions [4], which, thanks to their low melting point, provides a sort of self-lubricant effect.

Gane [5] and Wolfenden et al. [6] associated machinability improvement to the weak interface between the matrix and lead particles, promoting the formation of a Pb-thin monolayer. Alternatively, Johansson et al. [7] showed experimentally that lower cutting forces result from the Pb particles' deformation. The highly deformed particles elongate along the shearing plane, transitioning from spherical to flake-like structures within the brass matrix. This facilitates discontinuous chip formation as they act as crack initiation points. Therefore, the Pb-positive effect on brass's machinability is observed and supported by three significant observations: excellent chip breaking and control, low tool wear, and low cutting forces [8–10].

Pb-bearing brasses are prevalent in the manufacturing of diverse forged and extruded products, from automotive components to pipe fittings, keys, and locks [11]. However, despite the worldwide recognition of Pb being extremely harmful to human health [12–14], its use is currently still observed for components in direct contact with drinking water, which can be considered treacherous due to the potential for Pb's leaching [15].

Several organizations have issued regulations and guidelines to limit the maximum Pb content in brass components to address this hazard. Some examples are the EU Directive 2020/2184 of 16 December 2020 [16], which revises the maximum lead content in drinking water to 5 μg/l—half of the previous limit, which resulted in the creation of a dynamic list of alloys approved for use in contact with drinking water—the 4MS Common Composition List [17]. Other regulations have also been presented to control the maximum Pb content in different products/components, mainly for the automotive and electronic industries, and how these must be reported and managed as waste. Some examples of these directives and regulations are the Registration, Evaluation, Authorization, and Restriction of Chemicals (REACH) [18], the End-of-Life Vehicles Directive (ELV) [19], and the Restriction of the Use of Certain Hazardous Substances in Electrical and Electronic Equipment (RoHS) [20].

The brass industry operates within a closed-loop circular economy since its alloys are 100% recyclable [21]. Brass scrap recycling is crucial in reducing energy consumption, lowering the industry's carbon footprint, and providing a strong economic incentive by enabling the recovery of 75–90% of the alloys' original value [22]. Quantitatively, it is possible to state that brass production uses more than 90% secondary raw materials (scrap) [23]. However, given the increasingly stringent regulations on the Pb content, the brass scrap's circular economy can collapse due to the increasing difficulty in incorporating leaded brass scraps in the productive cycle [24].

From both economic and industrial points of view, the immediate substitution of lead by lead-free solutions is not cost-effective, due to high cutting tool wear and consequent difficult reincorporation into the life cycle [25]. Therefore, a compelling need to achieve innovative and productive machinable lead-free brass solutions persists. Considering this problem, the development of new lead-free brass alloys with a sustainability-based framework has become imperative.

This review article provides a systematic overview of current strategies for developing lead-free brass alloys with enhanced machinability, suitable for cost-effective industrial applications. Previous reviews have largely focused on qualitative descriptions of alloy compositions and processing methods, without offering a structured or quantitative comparison of machinability performance. This study addresses that critical gap by evaluating existing approaches through a consistent framework of machinability metrics, thereby enabling a more rigorous assessment of their practical suitability.

Methods

The present systematic review and analysis of the included studies were carried out according to the PRISMA 2020 guidelines [26] for conducting and reporting systematic reviews.

For this study, the Web of Science (WoS), Science Direct (SD), and Scopus (S) databases were used as sources of high-quality sample identification until February 26, 2025. The search query applied in each database is shown in Table 1. Additionally, alerts were set up to monitor the publication of new relevant articles, which were included if they met the inclusion criteria.

In addition to the search queries presented in Table 1, advanced filters available within each database were applied to refine the results. Specifically, records were limited to those of the following: (i) published from 2010 onward, (ii) written in English, and (iii) classified as original research articles (gray literature, reviews, and non-original publications were excluded). After duplicate identification and removal, title and abstract screening were undertaken by three researchers using the CADIMA web application [27] to screen the initially identified publications. A full-text examination was carried out for the final eligibility assessment.

Data extraction was undertaken independently by the same three researchers using a pre-piloted form in Microsoft Office Excel, followed by a group discussion. Data points included author, year of study, study objective and methodology, alloy compositions, study findings, and future work perspectives (if applicable). The PRISMA 2020 checklist for both manuscript and abstract is available as Appendix A and Appendix B, respectively.

Results

Based on the methodology employed, a total of 682 results were identified across the three selected databases. After duplicate identification, 114 studies were removed, leading to the title and abstract screening of 568 studies. From the screened studies, 93 studies proceeded to the full-text analysis. Figure 1 summarizes the overall identification and screening process.

From these 93 publications screened, it is possible to subcategorize them into three main categories for the development/tailoring of lead-free alloys through (i) alloying and particle/particulate additions, (ii) machining parameters optimization, and (iii) heat treatments, where 38 studies were selected for this review. 13 additional studies were also included to further analyze and enrich the study of

Table 1 Key search criteria

Context	Link	Keywords
Objective		"Brass" OR "copper-zinc" OR "Cu–Zn"
Constrain	AND	"lead-free" OR "Pb-free"
Application	OR	"Machining" OR "Machinability"

the high-entropy brass alloys (HEBAs) approach. From the screened publications, an analysis of the number of publications per year (Fig. 2a) and the occurrence of keywords (Fig. 2b) was carried out. The data indicate a predominant emphasis on alloy design approaches, while machining optimization and heat treatments are gradually attracting increased attention as researchers seek to enhance the performance of lead-free brass alloys for industrial applications. In the keyword analysis, a threshold of three occurrences was applied to the initial set of 140 keywords, resulting in 13 keywords meeting this criterion. As shown in Fig. 2b, "lead-free brass" and "machinability" are both highly represented and strongly interconnected, highlighting their central relevance to the selected research domain. The terms "microstructure," "mechanical properties," "chip formation," and "surface roughness" emerge as the most frequently employed evaluation criteria in the development of such alloys. In opposition, heat treatments are comparatively underrepresented, suggesting that future investigations could benefit from a more in-depth exploration of their role in improving machinability and overall alloy performance.

Discussion

As previously stated, the Pb's role during machining mainly consists of the deformation of spherical particles into needle-like structures, which will act as crack initiation points. Thus, the principal approach for the development of novel lead-free alloys has been focused on the formation of low-melting-point and/or soft precipitates

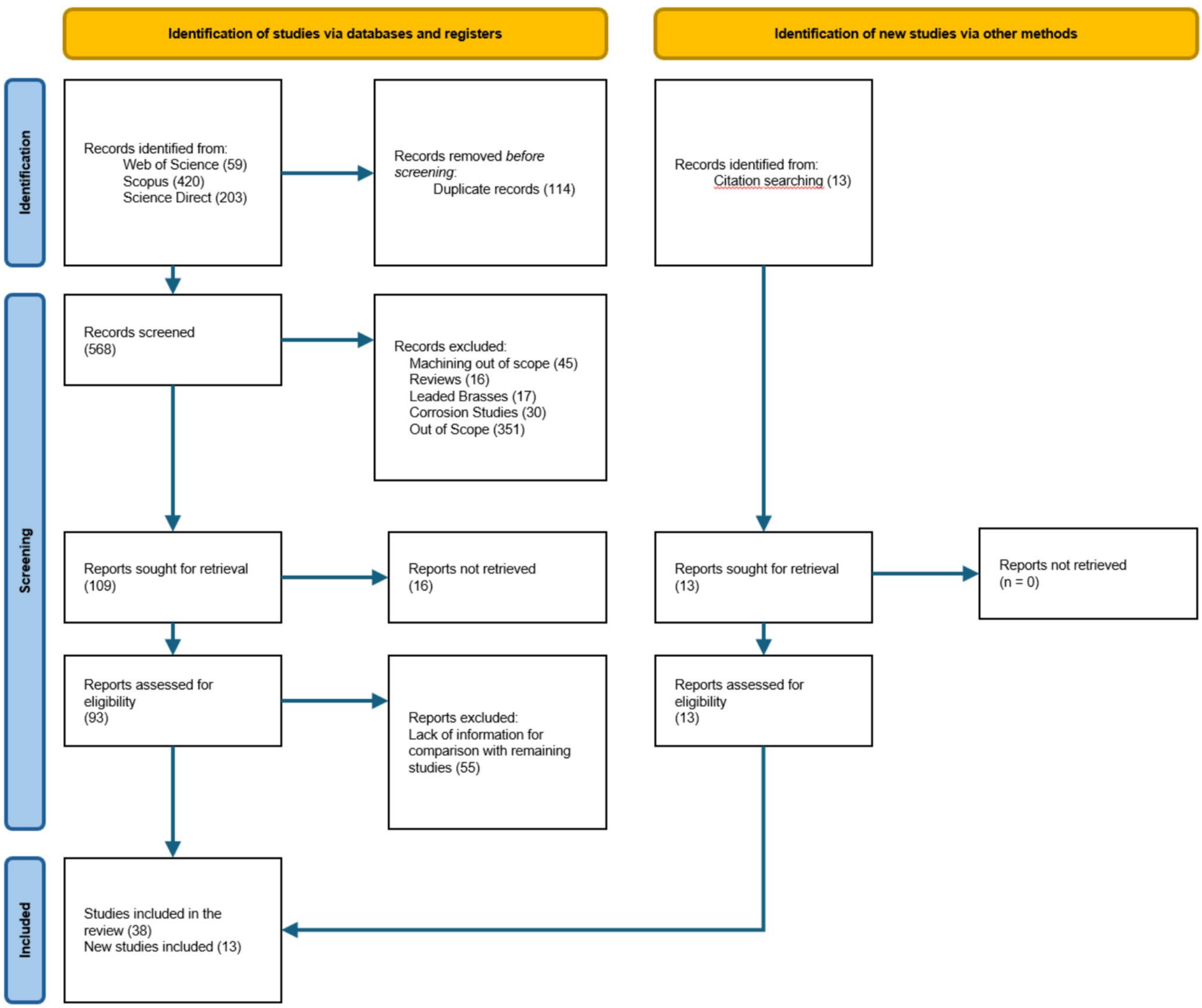

Fig. 1 PRISMA flow diagram of the study selection process [26]

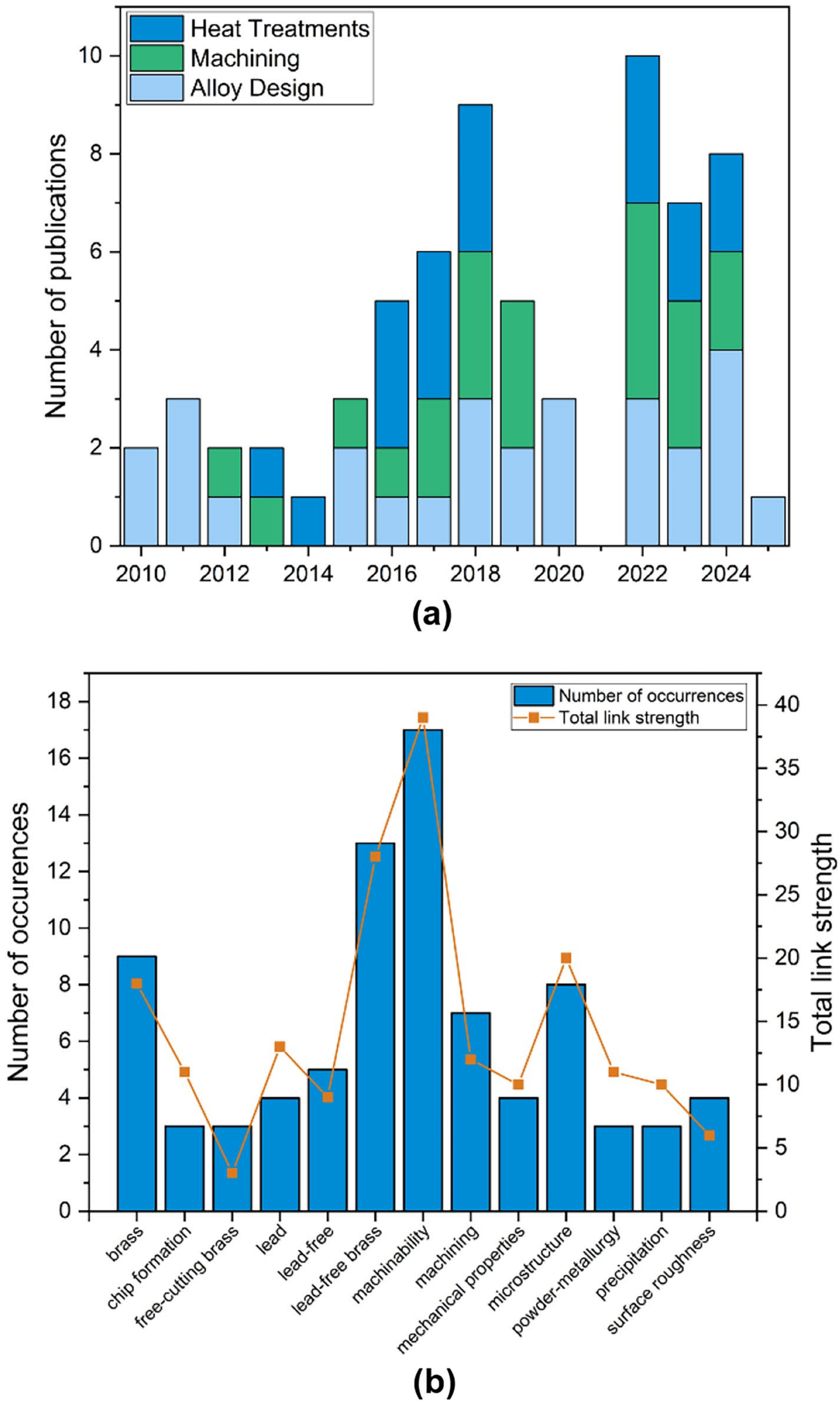

Fig. 2 **a** Year of publication distribution of the selected articles and **b** keywords analysis

that could replicate the Pb's morphology evolution during machining [28].

The brass matrix is also highlighted as a relevant characteristic to evaluate. The Cu/Zn ratio of conventional brasses mainly dictates the final alloy's matrix. Due to the minimal atomic size difference between Zn and Cu (~ −4%), a maximum solubility of ~ 35 wt% Zn in Cu's face--centered cubic (FCC) structure, known as α phase, is verified, leading to an efficient solid solution strengthening effect [29–31]. Single-phase α-brasses exhibit a considerably lower ultimate tensile strength (UTS) (< 350 MPa), when compared with other brass classes, alongside a significant elongation (> 30%). However, a higher corrosion resistance is observed due to high Cu content [29, 31]. For higher amounts of Zn (35 < Zn wt% < 45), at room temperature, the formation of an ordered body-centered cubic phase (BCC), known as β’ phase, is also observed, producing the alloys known as duplex brass. The peritectic reaction, $L + \alpha \rightarrow \beta$, at approximately 903 °C, justifies the formation of this dual-phase structure. However, it is essential to note that the solidification path does not end with the peritectic reaction mentioned above; with the decreasing temperature, a disorder-order transformation of the β (BCC_A2) to a β’ (BCC_B2) structure is observed [32]. At room temperature, the deformation potential of these alloys is limited owing to the hard β’ phase, which also reduces the corrosion resistance of duplex brasses when compared to single-phase α-brass alloys. The formation of such microstructural features increases UTS (> 350 MPa) at the detriment of elongation (40–10%) and corrosion resistance. Therefore, duplex brasses are usually heat-treated to minimize the presence of such microstructural features [29, 31]. The previously described phase transformations can be better understood through the analysis of the Cu–Zn phase diagram, as shown Fig. 2.

Due to the versatility of brass alloys, depending on the final application, a single-phase α-brass alloy may be required to ensure a superior corrosion resistance (e.g., sanitary applications), or a duplex brass may be necessary for superior mechanical performance (e.g., automotive applications). Thus, the alloy’s matrix may be adjusted to the final purpose. Nonetheless, Pb-like precipitates or particles are essential to enhance machinability, whether generated through alloying with additional elements or by the ex situ or in situ incorporation of alternative reinforcing phases. Other approaches are also found in the current literature, such as optimizing machining parameters and tailoring microstructures through heat treatments.

Current Commercially Available Alloys

Brasses are widely used, yet two main applications stand out: plumbing components or other kinds of components in direct contact with water, and automotive components. Based on each application, two distinct groups of alloys can be found, mainly dezincification resistance brass (DZR) and free-cutting brass (FCB), respectively. According to the ISO 6509 standard [34], DZR is an alloy with a maximum dezincification depth below 100 µm and 100–300 µm for forged and extruded products, respectively. FCB corresponds to alloys capable of high-speed machining with minimal tool wear and smooth surface finishes [35].

As an attempt to compare the alloys’ machinability, a quantitative machinability index is utilized. This parameter considers several factors: tool life, surface finish, chip formation, cutting forces (often presented in the form of power consumption), and metal removal rate. Therefore, the machinability index can be calculated as a relative percentage of any previously stated variable to the free-cutting brass CuZn38Pb3 (CW614N), which is assigned a value of 100% [36, 37]. Despite the clear distinction between these two groups, some alloys can present both DRZ and FCB characteristics, such as CuZn36Pb2As (CW602N) alloy, where a low dezincification depth is paired with a high machinability index (~ 80%).

With the removal of Pb from these alloys, a decrease is observed in the machinability index to less than 50% for Pb wt% < 1, resulting in a considerable decrease in productivity and an increase in manufacturing costs in alloys such as CuZn38As (CW511L) and CuZn42 (CW510L). Si-brass CuZn21Si3P (CW724R) was initially proposed as a novel lead-free brass for both applications, but failed to achieve the intended machinability, as it will be discussed in the following section. The relationship between the machinability index and the Pb wt% content, as previously stated, is shown in Fig. 3.

Regarding mechanical properties, ultimate tensile strength (σ_{UTS}), yield strength (σ_{YS}), and elongation (A), the current leaded and lead-free solutions present overall similar performances. However, when comparing the lead-free alloys, a general hardness increase and ductility are observed with the improvement of the machinability index, as observed between the CuZn42 and CuZn21Si3P alloys (Table 2).

Without Pb particles, these alloys rely on an increased dispersion of harder phases such as β,’ κ, and γ to assist the chip breaking mechanism, but it comes with a trade-off of lower ductility and increased wear of cutting tools, making it crucial to investigate machinable and cost-effective lead-free solutions.

Machining Parameter Optimization

Machinability is one of the characteristics most affected by Pb restrictions. Therefore, the pursuit of novel machinable alloys and the understanding of the influence of machining parameters on machinability, including these characteristics, have been at the forefront of research. However, the study of different cutting tools, as an alternative or complementary path, has also been explored [41, 42]. Nonetheless, machinability is not easily assessed due to the complex interaction between different machining parameters and material behavior, leading to a focus on machining parameter optimization itself.

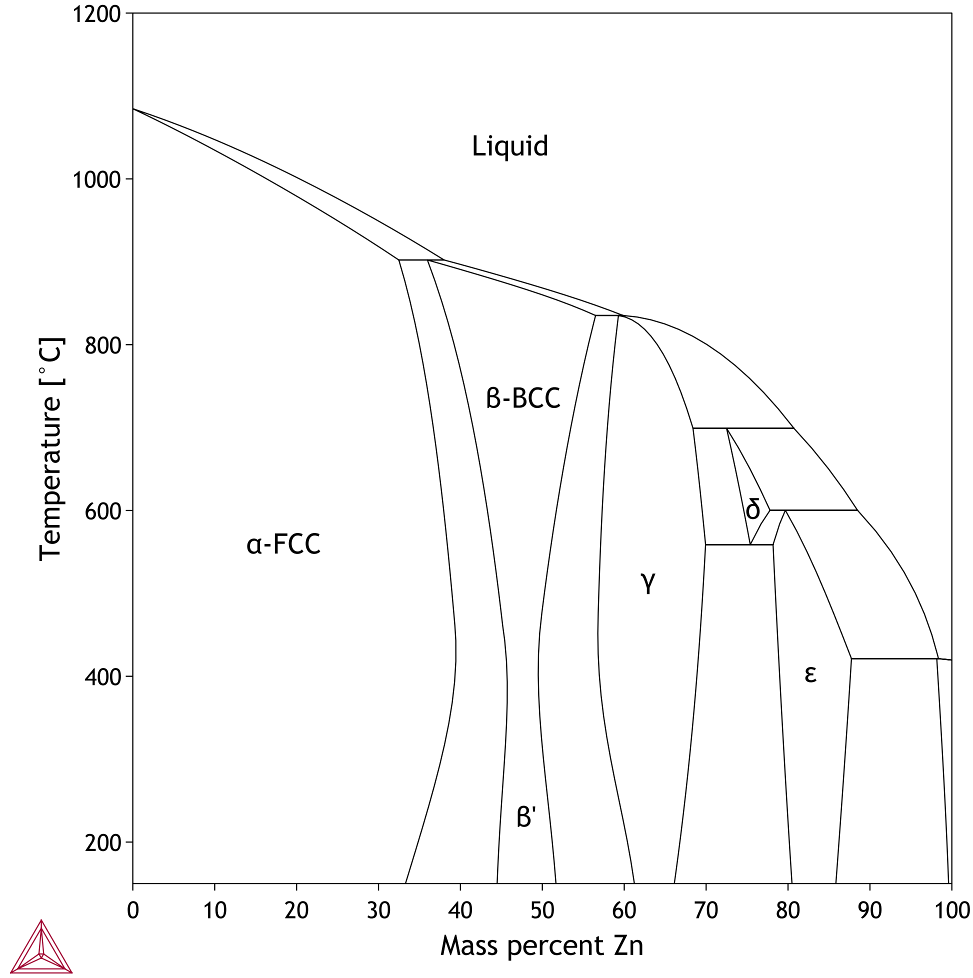

Fig. 3 Cu–Zn equilibrium phase diagram. Simulated with Thermo-Calc software [33]

Table 2 Benchmark of current leaded and lead-free market solutions

Alloy designation		σ_{UTS} [MPa]*	σ_{YS} [MPa]*	A [%]*	HBW	Microstructure	Machinability index [%]	References
CuZn38Pb3	CW614N	360	220	20	90—135	α + β' + Pb particles	100	[38–40]
CuZn36Pb2As	CW602N	280	200	30	70—135	α + Pb particles	80	
CuZn35Pb1.5AlAs	CW625N	280	200	30	70–135	α + Pb particles	55	
CuZn38As	CW511L	280	200	30	70–135	α	30	
CuZn42	CW510L	360	220	20	90—160	α + β'	50	
CuZn21Si3P	CW724R	500	300	15	130—220	α + κ + γ	80**	

*Minimal values for each alloy/property according to EN 12164. **Recommended the use of a chip breaker during machining operations

Nobel et al. [43] conducted an extensive study on the influence of material properties, Pb content, and tool design in chip formation and breakage during machining operations. In this work, three different alloys were used (CuZn38As, CuZn41.5 and CuZn21Si3P), with five lead contents tested (0.003, 0.011, 0.05, 0.19, and 1.9 wt% Pb) for the CuZn41.5 alloy. Machinability assessments were carried out through free orthogonal cutting tests in two stages: (1) varying the cutting speed (v_c) from 25 to 150 m/min while maintaining a constant feed of 0.2 mm and (2) varying the feed force from 0.1 to 0.4 mm with a constant v_c of 150 m/min. As expected, with the increase of Pb content, lower shear strengths were observed, allowing for more efficient chip breakage. For low v_c (25 m/min), no alloy with a Pb content below 0.19 wt% exhibited chip breakage, highlighting the Pb influence in the machinability of brasses. Regarding cutting forces, it was observed that a general decrease occurred until.

100 m/min, where the biggest decrease (~26%) was observed for the CuZn38As alloy. When comparing the different CuZn41.5 alloys, the researchers concluded that the increase in β'-phase fraction, justified by the Cu substitution for Pb, promoted a decrease in cutting forces and an increased chip breakage.

Johansson et al. [7] studied the effects of lead content on cutting forces (F_c) and friction coefficient (μ_r), using a constant depth of cut (a_p) of 2 mm in turning tests. For this work, two different alloys were selected, CuZn42 and CuZn38Pb3. The lead-free alloy presented a constant friction coefficient in the range of v_c and feed rate (f) employed. On the contrary, the friction coefficient of the CuZn38Pb alloy was considerably fluctuating from 0.2 to 0.55. Through the analysis of cutting forces for each f used (0.1, 0.2, and 0.3 mm/rev), it was found that cutting forces are mostly independent of the v_c. Comparing the studied alloys, the lead-free alloy exhibited higher cutting forces than the CuZn38Pb3 alloy, indicating lower machinability, as expected.

As an attempt to correlate the alloys' composition with both cutting forces and v_c, the experimental data from the above-mentioned studies [7, 43] were plotted as shown in Fig. 4. For this assessment, the f was fixed at 0.2 mm/rev, allowing for a more accurate comparison. Firstly, as expected, highly leaded alloys (CuZn39Pb3) exhibit low cutting forces for the whole range of v_c studied. Yet, beyond 50 m/min, the cutting force tends to stabilize, suggesting that at higher v_c, cutting forces become largely independent of such a variable. In contrast, other alloys show more varied behavior, with some displaying gradual decreases or fluctuations, but a general decrease in cutting force.

Besides the β-phase ratio and Pb content, several parameters regarding the machining operation are believed to influence machinability. Tascioglu et al. [44] evaluated surface integrity by correlating cutting forces generated during machining with surface deformation. Similar cutting forces were observed for cutting speeds of 200 m/min and 400 m/min, validating a possible stabilization of cutting forces for high cutting speeds. Yet, it was reported that the lowest cutting forces (106, 191, and 160 N for the CuZn40Pb2, CuZn38As, and CuZn21Si3P alloys, respectively) were obtained for the lowest f studied (0.1 mm/rev). Overall, with the f increase, from 0.1 to 0.25 mm/rev, at least an 80% increase in cutting force is observed for all the alloys and, alongside this phenomenon, a surface roughness increase of more than 180% is also present. The machined specimens had a significant increase in hardness up to a 100 µm depth from the surface (37%, 84%, and 49% for the CuZn40Pb2, CuZn38As,

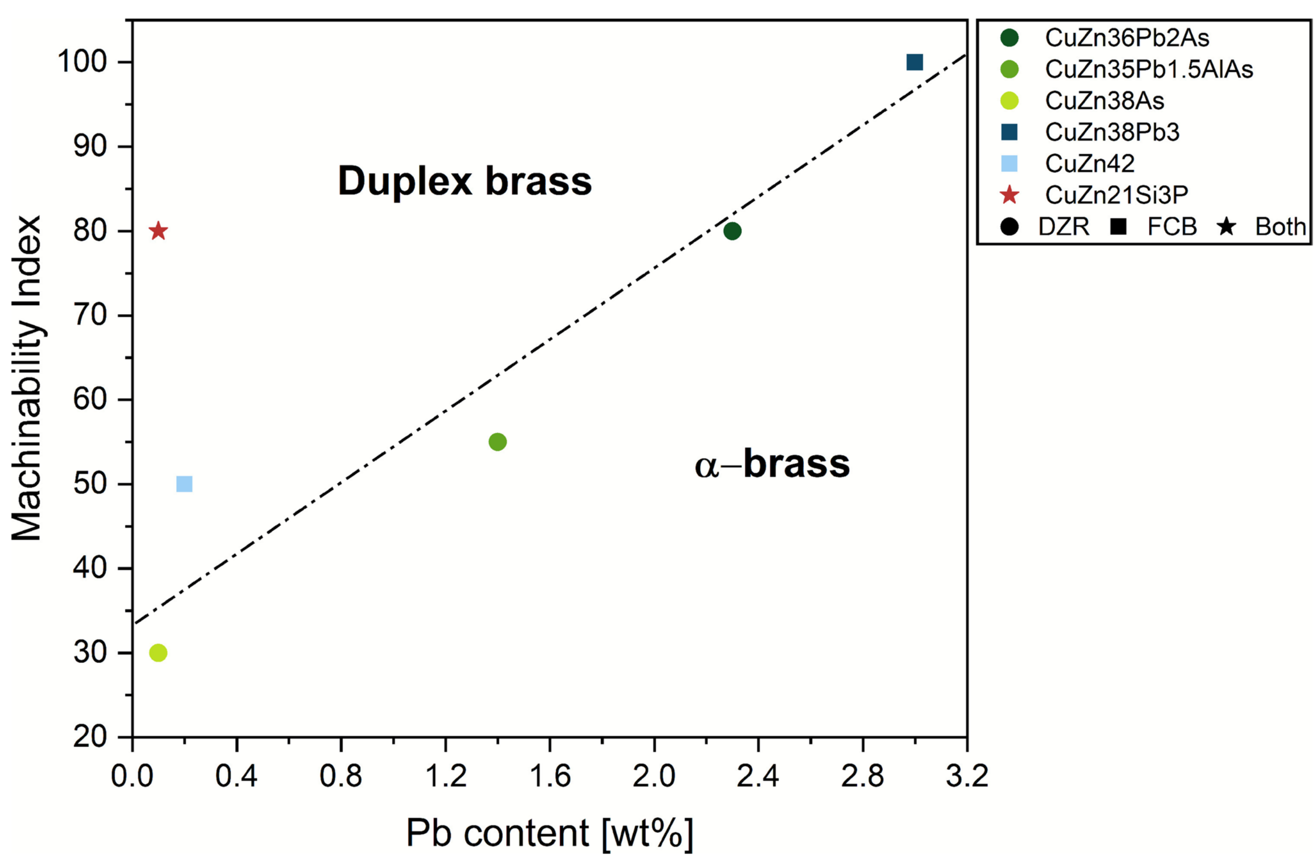

Fig. 4 Machinability index evolution with the Pb wt% content [38–40]

and CuZn21Si3P alloys, respectively), paired with twin formation for the low- and lead-free alloys; however, no further investigations were carried out regarding the role of such subsurface deformation on the machining performance.

In an attempt to statistically optimize machining parameters, Das et al. [45] studied the machinability of lead-free brass components with ANOVA after the experimental machining trials were carried out. High-speed micro turning tests were performed by varying v_c (25, 100, and 175 m/min), f (3, 6, 9, and 12 µm/rev) and a_p (30, 40, 50, and 60 µm), allowing its correlation with both surface topography, burr height (height related to the raised edge of material on the specimen edges formed after machining operations), and chip formation.

The statistical analyses highlighted the general contribution of v_c for both average surface roughness and burr height, where its contribution was 56.86% and 64.61%, respectively. The increase in surface roughness with increasing cutting speeds was primarily attributed to lower friction, smaller uncut chip thickness, and overall work hardening of the specimen. Despite burr height not being a commonly assessed parameter in machining studies for brass alloys, it was observed that the increase in burr height could be associated with the difficult chip breakage, induced by lateral plastic deformation of the workpiece during machining. As expected, the chip breakage was unfavorable due to the rapid plastic deformation of the lead-free alloys' matrix.

In addition to the parameter complex interaction and contributions, objective functions were obtained through regression analysis, allowing for the prediction of workpiece characteristics. Based on this analysis, the most attractive combination of process parameters was v_c equal to 125 m/min, f of 3 µm/rev, and a a_p of 40 µm. This approach could be implemented for a quicker process optimization in industrial environments, since larger amounts of data (from compositions, processing conditions, etc.) could be added for a more accurate prediction.

Toulfatzies et al. [46] conducted a study with the goal of optimizing the main cutting force by investigating its correlation with a_p, f, and v_c, through the Taguchi method and an ANOVA. This approach allows for the consideration of complex and multiple interactions between the studied parameters, resulting in a more accurate process optimization.

Thus, since one of the variables considered in the presented design of experiments (DoE) is the materials' chemical composition, the optimal solution for minimizing cutting forces was the Pb-richer alloy, CuZn39Pb3 alloy. The optimal parameters for this alloy were established when paired with a v_c of 247 m/min, an a_p of 0.5 mm and a f of 150 mm/min. Therefore, it is considered a more relevant and accurate approach for process optimization, the construction of a DoE for each alloy, allowing for the process optimization specific to an alloy/application. Additionally, the ANOVA revealed that v_c plays a minimal role (~3.6%) in the cutting force, while a_p is the parameter that influences the final main cutting forces most (~64.4%). Regarding the surface roughness optimization, the lowest value was determined for a v_c of 1750 rpm, an a_p of 0.5 mm, and a f of 150 mm/min for the CW511L alloy. Based on the ANOVA, f is the main parameter influencing the final roughness (~55.3%).

This approach for optimization can allow for performance tailoring based on complex interactions between parameters. Furthermore, it is possible to define multiple objectives through these advanced statistical approaches and determine the ideal solution based on the balance between single-parameter optimization; therefore, they should be highly utilized for future research on machining parameter optimization.

Table 3 summarizes the key findings of the studies analyzed in Sect. "Machining Parameter Optimization". The vast range of machining parameters significantly hinders the comparisons between studies, and the lack of consistent evaluation criteria also limits the assessment of the effect of isolated variables and alloy-specific findings. General guidelines should be defined based on machinability optimizations, using multiparameter statistical analysis paired with well-defined processing windows.

Heat Treatments for Microstructure Design

Heat treatments have also emerged as a critical processing step for enhancing the machinability of lead-free brasses, alongside the optimization of machining parameters. Microstructure tailoring can be achieved by a precise control of heating and cooling cycles, inducing beneficial microstructural changes, such as the formation of a controlled amount of the β'-phase in predominantly α-phase matrices.

As previously mentioned, it is observed that both α-and duplex brasses tend to show higher machinability when higher amounts of β'-phase are present, due to their higher hardness when compared to the α-matrix. Toulfatzis et al. [47] studied the microstructural tailoring through several post-processing heat treatments in an attempt to promote the controlled growth of the β'-phase, while maintaining mechanical properties within the respective EN alloys' standard. In this study, three different alloys were considered: CuZn38As (CW511L), CuZn42 (CW510L), and CuZn36 (C27450), where three different temperatures (700, 775, and 850ºC) and three different staging times (15, 60, and 120 min) were used. Figure 5 shows the evolution of the β'-phase fraction and the hardness with the respective heat treatments. Generally, it can be stated that with the increase of both soaking time and temperature, the β-phase fraction increases because it becomes more stable at higher temperatures. This increase is pronounced for the CW510L alloy, due to its higher Zn content, which allows it to enter the

Table 3 Summary of Sect. "Machining Parameter Optimization" key findings

Alloys	v_C	f	a_p	Findings	Reference
CuZn38Pb3 CuZn42	20–200 m/min	0.05–0.3 mm	2 mm	As the Pb content increases, lower shear strengths are observed A general decrease in cutting forces occurs up to cutting speeds of 100 m/min	[7]
CuZn38As CuZn41.5 CuZn21Si3P	25–150 m/min	0.2 mm	0.4–0.8 mm	The leaded alloy exhibits an almost constant friction coefficient across the range of parameters evaluated, along with overall lower cutting forces	[43]
CuZn40Pb2 CuZn38As CuZn21Si3P	200, 400 m/min	0.1–0.25 mm	1 mm	An increase in feed rate results in at least an 80% rise in cutting force, accompanied by higher surface roughness	[44]
CuZn42	100–175 m/min	0.003–0.012 mm	0.03–0.06 mm	With increasing cutting speed, both the average surface roughness and burr height increase, which is associated with reduced friction during machining	[45]
CuZn42 CuZn38As CuZn21Si3P CuZn37	165–247 m/min	0.5–2 mm	150–500 mm/min	The depth of cut plays a critical role in the variation of cutting forces, while cutting speed has the greatest influence on surface roughness	[46]

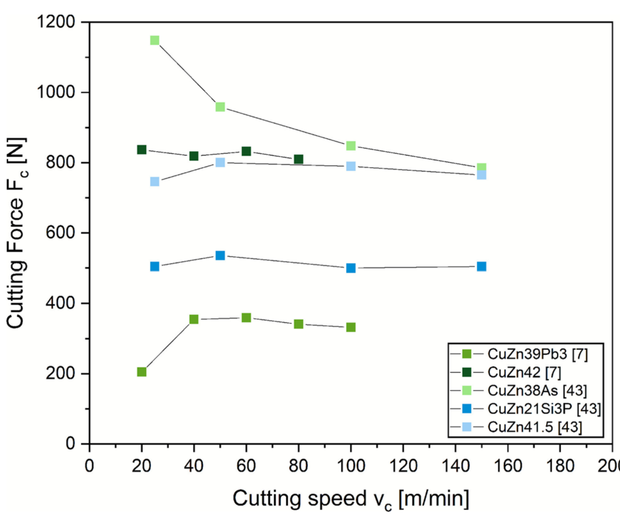

Fig. 5 Cutting force evolution with the cutting speed for different conventional alloys [7, 43]

fully β-phase domain at higher temperatures. In terms of hardness evolution, a slight decrease in hardness (~20–25%) is observed for the CW511L and C27450 alloys, associated with the α-phase grain size growth for the shortest soaking time. However, with the increase in both time and temperature, an increase in hardness is observed due to the β-phase formation. Grain size and aspect ratio, among others, were not covered, although recent studies have mentioned their influence on dezincification performance [48].

In a subsequent study, the same authors [49] assessed the machinability of each heat-treated alloy that presented the highest amount of β'-phase, this being the following: CW510L—775ºC for 60 min; CW511L—850ºC for 120 min; and C27450—850ºC for 120 min. Through turning operations, the chip morphology, power consumption, cutting force and surface roughness (Rt – "Peak to Valley") were assessed to fully understand the effect of these heat treatments on the final alloys' machinability. Table 4 summarizes the effect of heat treatments on each assessed parameter.

Overall, it is possible to affirm that the heat treatment was clearly efficient in improving machinability for the CW511L alloy, mainly explained by the microstructure tailoring into an almost duplex brass. However, it is important to consider that such an alloy is DZR. The obtained duplex structure reduces the alloy's dezincification resistance; therefore, it cannot be considered a solution for such applications. Regarding the remaining studied alloys, no significant alteration was observed in terms of cutting force, power consumption, or roughness. However, a clear change in the chip morphology was observed. A transition from a ribbon-like to a conical helical chip, for all the studied alloys, translates as a significant improvement of the machining conditions. This can be associated with the elimination of possible chip entanglement on the cutting tool, which can lead to additional manufacturing costs (increased machine down times, decrease of the tool life, etc.).

Brans et al. [50] researched the influence of the material production route on the machinability of lead-free brass CuZn40. By varying the amount of heat treatment and work hardening, four different samples of CuZn40 were produced from a previously extruded cylinder with a 10.3 mm diameter. The first specimen (V1) consisted of a cold-drawn sample with a diameter of 10 mm, while the second specimen (V2) had a higher degree of cold drawing, resulting in a sample with a diameter of 8 mm.

Table 4 Results of lead-free brasses before and after the selected heat treatment processes [48]

Material	Chip morphology*	Power consumption [W]	Cutting force [N]	Rt[µm]
CW510L	Class 4	1900	540	78.6
CW510L_HT	↑ **Class 2**	↓ **2020**	↑ **530**	↓ **79.5**
CW511L	Class 5	1600	446	40.1
CW511L_HT	↑ **Class 3**	↑ **1420**	↑ **431**	↑ **26.0**
C27450	Class 5	1390	346	49.2
C27450_HT	↑ **Class 3**	↓ **1460**	↓ **373**	↓ **59.4**

*Chip morphology classification according to ISO3685: 1 needle chip, 2 arc chips, 3 conical helical chips, 4 washer-type helical chips, 5 ribbon chips

The third specimen (V3) underwent similar processing to the second, except it received an extra heat treatment for 120 min at 500ºC. In the last specimen (V4), the heat treatment was the first step, conducted at 550ºC for 120 min, followed by cold drawing, resulting in a diameter of 10 mm. Figure 6 shows the microstructure for each variant produced.

The microstructure analysis verified that V1 and V4 present similar globular microstructures, while V2 and V3 present elongated β'-phase. Due to the final heat treatment, V3 did not present microstructural anisotropy. V1 and V4 presented similar phase fractions, with β'-phase representing 19% and 18%, respectively, while V2 presented the highest β'-phase fraction with 28%, and V3 had the lowest with 12%. Machinability evaluation revealed the role of harder phases (β'-phase) for machinability improvement. V1 and V4 presented similar behaviors, as expected by the previous microstructural and mechanical observations. Yet with the increase of the β'-phase fraction, it was observed that the lowest cutting force (784 N) was against the highest value (862 N) in V3, which presented the lowest β'-phase fraction.

Sathiskumar et al. [51] studied the effect of heat treatment on brass alloy 272 (CuZn37) and analyzed the variation in material removal rate (MRR) and surface roughness (Ra) to assess its influence on the alloy's machinability. ANOVA statistical analysis was employed throughout this work, enabling the correlation of several parameters with the respective outputs. The machining tests indicated an increase in MRR from 29.27 mm^3/s to 40.32 mm^3/s and an overall decrease in machining time for the heat-treated samples, improving the desirability value (a statistical parameter used to optimize multiparameter operations where 100% corresponds to the most desirable solution) from 54.6% to 71.9%. However, the absence of microstructure analysis, the description of the heat treatment, and the assessment of other relevant machining parameters (e.g., cutting forces) hinder comparison with other studies.

Two other studies [52, 53] addressed the optimization of the heat treatment for lead-free alloys; however, they did not

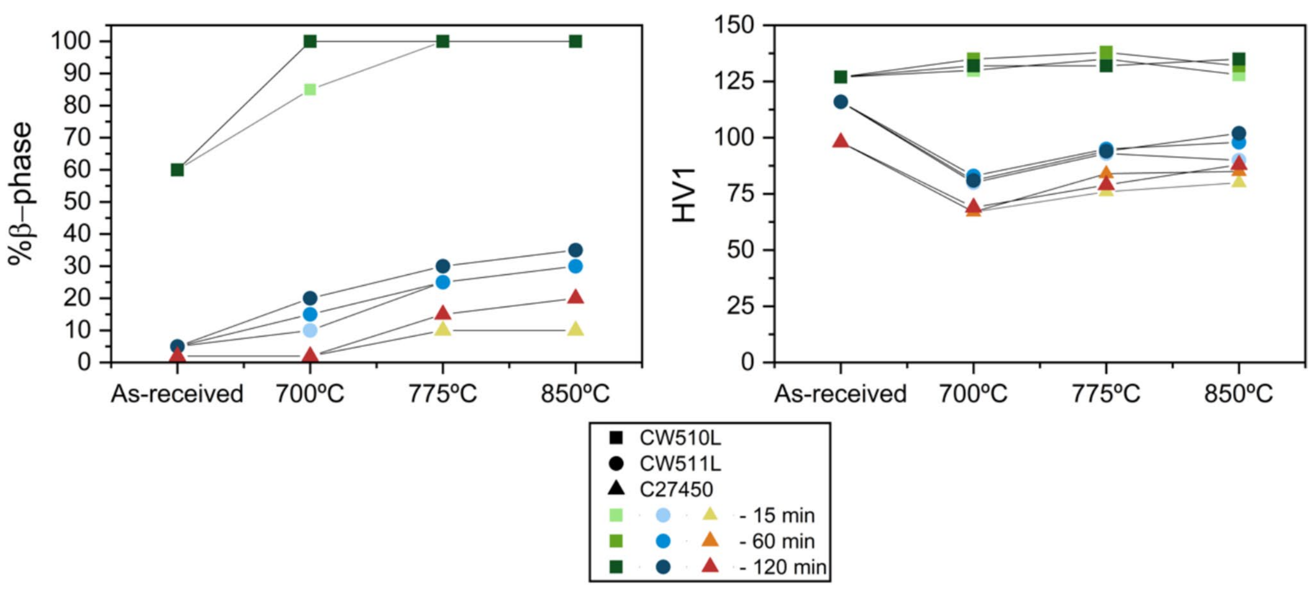

Fig. 6 Evolution of β'-phase fraction and hardness with heat treatments [47]

cover machinability evaluation (cutting force measurements, roughness, etc.), which also hinders the direct comparison with commercially available alloys and their further industrial acceptance.

An overview of heat treatment studies for lead-free brasses is shown in Table 5. Overall, it was possible to identify a significant variability in the experimental methodologies adopted across studies. Besides the expected variation in heat treatment temperature and holding time, which is normally defined based on the alloy's composition, a wide range of testing approaches, parameters, and evaluated criteria is observed. This heterogeneity poses a considerable challenge to the direct comparison and correlation of findings among studies.

For instance, while certain reports focus primarily on mechanical properties such as hardness, others assess machinability criteria, such as cutting forces or surface integrity parameters including roughness (Ra and Rt). The inconsistency in both the choice and definition of evaluated criteria complicates the identification of general trends linking heat treatment conditions to resulting machinability. Moreover, a variation in testing configurations and inconsistent machining parameters was identified. This methodology selection directly influences heat generation, tool wear, and surface finish, further limits the ability to derive unified conclusions, as these methods impose distinct stress and thermal conditions on the material. Altogether, the lack of standardized assessment protocols hinders the development of a coherent understanding of how heat treatment modifies the machinability of brass alloys.

Alloy Design

With the need for the removal of Pb from brass alloys, research has also shifted toward identifying alternative alloying elements and reinforcements to improve machinability. A key focus has been the introduction of soft intermetallic phases that replicate the effects of Pb particles in leaded brasses.

The incorporation of graphite was initially proposed by Imai et al. [54] in the Cu-40Zn brass through powder metallurgy (PM). The brass composite presented a homogeneous microstructure with graphite particles, where no significant dissolution of carbon into the brass matrix (α and β-phases) was observed, and a similar volume fraction of Pb particles in a 3.2 wt.% Pb conventional brass. Despite the poor interface bonding between the matrix and graphite particles, drilling times similar to those of leaded brass (10 s) were achieved, incorporating 1 wt.% graphite (20–15 s), displaying a lubricant effect of graphite soft particles. To improve mechanical and machining performance while enhancing interface bonding of brass/graphite particles, Ti additions were studied by Zhang et al. [55]. However, with the increase in Ti content, the formation of Cu_2Ti_4O particles and Ti nanoclusters increased gradually, deteriorating alloy ductility up to ~ 35% with the addition of 1.9 wt.% Ti, despite improving machinability (~ 16% decrease in cutting forces). This phenomenon may be associated with the solid solution strengthening and the formation of nanoprecipitates. Imai et al. [56] also studied the combination of graphite and Bi addition to the Cu-40Zn brass through PM, since both additives present a low solubility in the Cu–Zn matrix. Through SEM–EDS analysis, it was shown that Bi-islands and graphite islands formed separately. These

Table 5 Summary table of the heat treatment studies analyzed

Material	Heat treatment		Type of test	f	a_p	Evaluated criteria	Reference
	T [ºC]	t [min]					
CuZn38As – CW511L CuZn42 – CW510L CuZn36 – C27450	850 775 850	120 60 120	Cylindrical Turning	150–500 mm/min	0.5–2.0 mm	β-phase fraction; Power consumption; Cutting Force	[47, 49]
CuZn40 (cold draw) CuZn40 (cold draw after HT)	500 550	120 120	Orthogonal Cutting	25; 150 m/min	0.01; 0.5 mm	β-phase fraction; Cutting Force; Chip Classification; Roughness – Rt	[50]
CuZn37	(not disclosure)		Cylindrical Turning	0.1–0.3 mm/rev	0.5; 1; 1.5 mm	Material Rate Removal; Roughness – Ra	[51]
CuBi0.6Zn29 (homogenization, followed by deformation and annealing)	800 350; 400; 450	120 15	-	-	-	Hardness	[52]
CuZn21	300; 400; 500; 600	15	-	-	-	Hardness	[53]

microstructural features allowed for the approximation of the lead-free machining time (between 10–20 s per 5 mm-depth hole) to drilling times for leaded brass (consistently around 10 s per 5 mm-depth hole); however, a significant decrease in ductility (from less than ~ 20 to ~ 50%) was verified. In contrast to the previous study, Li et al. [57] demonstrated that the incorporation of small amounts of Cr, Fe, Ti, and Sn (0.7, 0.3, 0.6, and 1 wt.%, respectively) promoted grain refinement by the precipitation of nanoprecipitates while strengthening the graphite/brass interface. This combination of graphite reinforcements and grain refiners enabled the development of an alloy with high σ_{UTS} (~ 700 MPa), good performance of machinability (60–80% of leaded brass machinability), and acceptable ductility (~ 12%). Building on the concept of replacing Pb with graphite particles, Zhou et al. [58] proposed cast brasses containing cementite particles (Fe_3C), in situ formed by the incorporation of cast iron scrap, followed by graphitization annealing. This approach facilitated the in situ formation of graphite particles, thereby eliminating the possible risk of graphite particle flotation in the melt, and highlighting structural similarities between cementite and short-range atomic group ordering in melts. Machining tests revealed improved chip segmentation and lubrication compared to conventional lead-free brass alloys; however, no further investigation was carried out into the mechanism of graphite particles for improved machinability. Despite several efforts to develop graphite reinforced brasses, the lack of interface bonding with the matrix, the technical complexities, increased associated costs with processing methods, and regulatory obstacles linked to non-standard alloy compositions are still drawbacks to the industrialization of such technology.

Another highly investigated approach uses Si as a stabilizer of β and β′ phases, moving the peritectic reaction to lower Zn content and higher temperatures. Doostmohammadi et al. [59] studied the Si influence, up to 1.7 wt%, on the microstructure and hardness of a Cu-40Zn brass. The initial duplex brass transforms into a fully β′ microstructure with the addition of 1.2 Si wt%, while also achieving grain refinement of ~ 80% of the initial grain size. Thermodynamically, the authors demonstrated that the electron-to-atom ratio (*e/a*) increases with the Si content, thereby decreasing the stacking fault energy (SFE) and favoring the formation of β-phase. Additionally, due to the hardness increase with the Si content, a machinability improvement of the initial alloy was predicted. However, no experimental machinability evaluation was performed. Oishi et al. [60] and Sasuki et al. [61] employed the same Si-alloying approach to a duplex brass with 1 wt.% Si. These studies proved that, with an increase in the Cu content (62.5 wt.%), this approach could develop machinable lead-free brass alloys, depicted by the low cutting forces and sound chip breaking mechanism, with similar mechanical performance (σ_{UTS}, σ_{YS} and A of 580 MPa, 415 MPa, and 25%, respectively). Schultheiss et al. [62] proceeded to study the machinability of Si-brass alloys in more detail. Besides the clear differences in σ_{UTS} and σ_{YS} between the leaded (525 and 201 MPa, respectively) and the lead-free alloy (717 and 342 MPa, respectively), the abrasiveness of the Si-brass was 1.6 times higher, leading to a shortened tool service life during machining operations. This phenomenon was confirmed by increased cutting forces from 220 to 300 N, increased cutting resistance from ~ 1500 to ~ 2000 MPa, and a longer chip length.

Taha et al. [63] also showcased the formation of γ-phase as small precipitates at the grain boundaries alongside other microstructural features; however, with a 4 wt.% Si addition, an almost duplex β' + γ brass alloy was obtained. Additionally, the presence of Si allowed the formation of other brittle phases, such as κ-HCP and ε-$Cu_{15}Si_4$, promoting an overall strength reduction and an increase in both tool wear and final roughness. Despite the clear drawbacks of Si-brasses, these alloys are still presented as one of the few commercially available lead-free solutions.

Beyond traditional alloying methods, recent research highlighted the potential of composite reinforcement as an effective strategy for enhancing both the machinability and mechanical performance of lead-free brasses. This approach relied on the incorporation of reinforcements that could replace the role of Pb during machining or promote the formation of new microstructural features that could perform that role. Clinktan et al. [64] studied the incorporation of boron carbides (B_4C) into a silicon brass CuSi4Zn14; however, despite the grain refinement effect and increase of grain dislocations, no machining study was carried out to assess the suitability of such a developed composite. Peng et al. [65] proposed the reinforcement with Ti_3AlC_2 particles. Initially, the β'-phase fraction would increase with the reinforcement content increase due to the Al diffusion during sintering. Regarding mechanical performance, an increase in hardness (~ 150%), bending strength (~ 47%), paired with a decrease in the wear constant (~ 70%), was shown with the incorporation of 5 wt% of Ti_3AlC_2. However, the wear resistance increase could not represent a universal improvement, since it could also be translated into a shorter tool life during machining operations.

Semih et al. [66] proceeded to the reinforcement with two different additives, Si and molybdenum disulfide (MoS_2), since both are widely available commercially and are far less toxic than Pb. With the increase of MoS_2, there was an increase in the β'-phase fraction, leading to both hardness and tensile strength increase, while decreasing the alloys' ductility. Machinability trials demonstrated that brittle intermetallics promoted a more effective chip breaking mechanism, while exhibiting a significant lubricating effect, as shown by the ~ 78% decrease in overall Ra.

In addition to this novel approach to alloy design, several studies have been conducted through more conventional design approaches, such as the addition of small amounts of other alloying elements. Rajabi et al. [67] assessed the effect of Sn on the microstructure and machinability of Cu-30Zn brass alloy. It was shown that a transition from a duplex brass into a fully β'-brass occurred, and for the highest Sn contents, 11.4, 13.9, and 17.4 wt%, the formation of γ-phases was observed. In addition to the hardness increase, promoted by the formation of β' and γ-phases, a grain refinement effect was also observed. Suksongkarm et al. [68] combined Sn and Bi additions through a sustainable approach, resorting to recycled Bi-Sn solder alloys. Identical microstructural evolutions were observed; however, with the Bi addition, spherical Bi-rich particles were also present. With this combination, machining forces decrease (around 40%), and favorable, shorter chips were obtained, presenting this as a viable approach. Similarly, the study of Atsumi et al. [69] demonstrated the synergetic effect of Cr and Fe on the previously studied alloying elements. These additions facilitated the formation of Cr-Fe intermetallics and Bi particles, enabling the achievement of 75% of the machinability typically associated with leaded brass. However, the absence of chip morphology characterization and surface roughness data hinders direct comparison with other studies on the machining performance.

The main shortcoming in the current literature regarding the development of lead-free brasses lies in the lack of comprehensive information on their machinability. In addition, there is a general inconsistency in the methodologies used to evaluate machinability, with variations in cutting conditions, tool materials, and evaluation criteria. These discrepancies make it difficult to perform a reliable quantitative comparison between different alloy compositions. For instance, different studies [70, 71] investigated the influence of Ti, and Ti in combination with Sn, on the microstructural evolution and mechanical properties of 60/40 brass produced via PM. Chen et al. [72] examined the formation and impact of Ni_2Si precipitates through the alloying of Ni and Si, while Li et al. [73] evaluated the incorporation of Fe-rich scrap and Al to promote the development of iron-based precipitates. Although these studies present innovative approaches for the design of lead-free brass alloys, mainly by the formation of different precipitates that could replicate Pb's role, machinability remains unassessed. This is a critical parameter for industrial implementation and subsequent commercial viability.

In contrast with the previously presented studies, some studies are highlighted due to their systematic evaluation of crucial properties. For example, two different studies from Adineh et al. [74, 75] evaluated the effect of Mg, Sb, Si, and Al through a consistent and complete approach, comprising microstructural, mechanical, and machinability assessments. With the increasing alloying element content, the β'-phase fraction increased, and for high contents of Mg and Sb, the formation of other intermetallic structures was observed. On the other hand, higher Si contents (greater than 1.87 wt.%) promoted the stabilization of the γ phase. Paired with the formation of such phases, a hardness increase (2.88 × the initial value) was observed. Regarding machinability, the assessment of the three cutting force components: main cutting force (F_c), thrust force (F_t), and feed force (F_a), through a piezoelectric dynamometer, allowed the calculation of the resultant cutting force (F_m) through Eq. 1.

$$F_m = \sqrt{F_c^2 + F_t^2 + F_a^2} \tag{1}$$

With this approach, not only were the tool wear and chip breaking mechanisms analyzed, but also the resultant cutting force necessary to produce the intended machining. It was shown that overall, Mg and Sb significantly increase the cutting forces during machining operations. On the other hand, up to 2 wt% Al and 1 wt% Si promoted a machinability improvement, with a decrease of 10–34% and 28–37% in the cutting forces, respectively. To compare the previously presented machining studies, the F_m was plotted against the main alloying element (Fig. 7). Generally, a decrease in the resulting force is observed for all the alloying element contents, except for Si and Al. The behavior of Si and Al could be associated with the formation of harder phases. To better isolate the influence of each alloying element, more precise comparative methods—such as calculating the specific cutting pressure (Kc) — would be advantageous, as they help eliminate the impact of machining parameters like a_p and v_c. [76]. On the other hand, it is observed that most of the studies limit alloying element addition to 4 wt%. This could represent a new opportunity window to study the potential benefits of larger alloying additions (> 5 wt%) for the development of alloys with improved machinability and overall performance.

To illustrate the variability of machining parameters employed, two separate tables—Tables 6 and 7—are presented as an overview of the selected studies, encompassing composition, parameters, and evaluation criteria. From the identified drilling studies (Table 6), it is evident that the same type of tool and certain parameters were consistently used; however, the evaluation criteria are less comparable due to differences in machining operations, and no chip classification was reported. In contrast, Table 7 summarizes turning studies and those that did not explicitly assess machinability. In these cases, chip classification appears as the most frequently used criterion for evaluating machinability. Overall, the wide variation in v_c, f, and a_p hinders direct comparison between studies in which cutting forces were measured, as each parameter combination promotes distinct machining responses, as previously discussed.

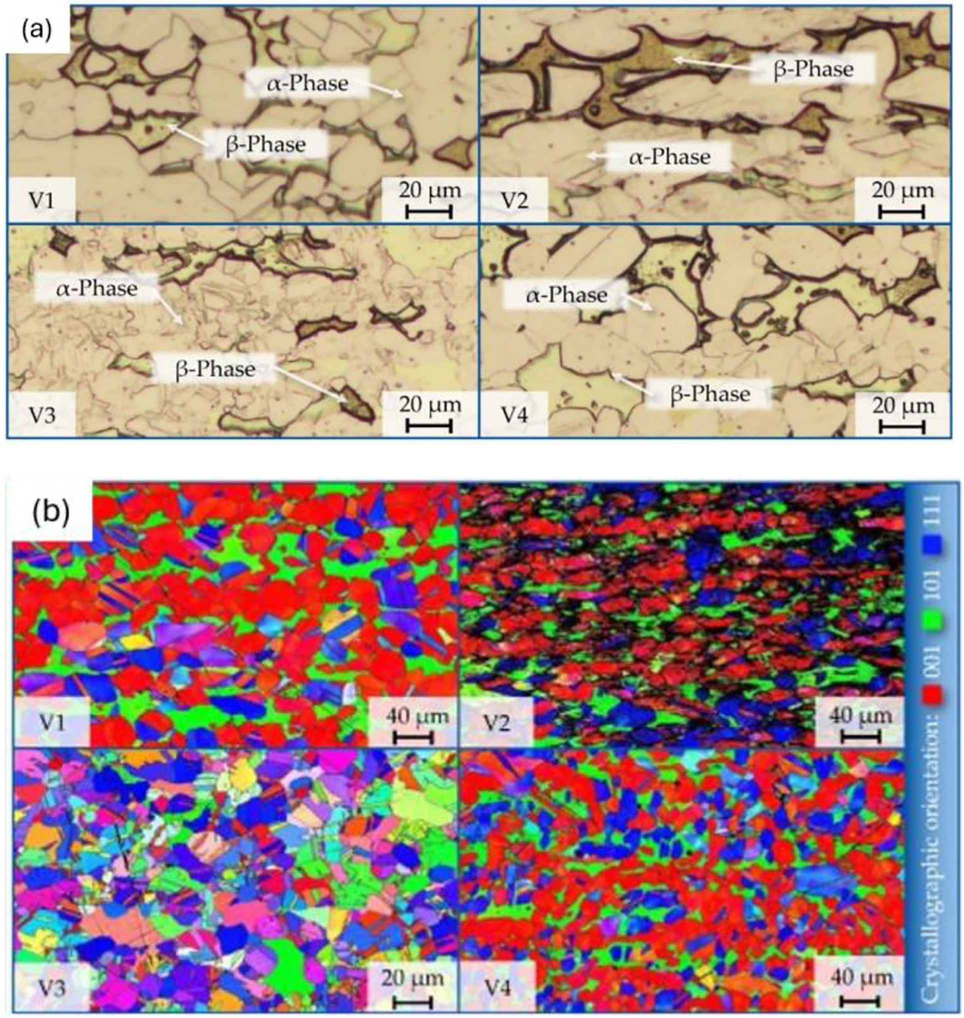

Fig. 7 **a** Optical microscopy images and **b** EBSD inverse pole figure maps for each material variant. Adapted from [50]

Table 6 Overview of drilling studies

Addition	Amount	Base Alloy	Type of test	Drill diameter	RPM	Force	Evaluated criteria	Reference
Graphite	Up to 1 wt.%	CuZn40	Drilling	4.5	900	9.8 N	Time to produce a 5 mm-depth hole	[54]
Graphite + Bi	Graphite: 0; 0.25; 0.5 wt.% Bi: up to 3.3 wt.%	CuZn40	Drilling	4.5				[56]
Cr, Fe, Ti and Sn	0.7, 0.3, 0.6, and 1 wt.%, respectively	CuZn40	Drilling	4.5		14.7 N		[57]
Bi	Bi: up to 3 wt.%	CuCr0.3Fe0.2Sn0.6Zn40	Drilling	4.5		98 N		[69]

Another promising avenue for alloy design has been the application of medium-entropy alloy (MEA) or high-entropy alloy (HEA) design concepts to brass systems. The HEA concept was first introduced by two independent researchers, Cantor [77] and Yeh [78], at the beginning of the twenty-first century, primarily motivated by a desire to advance metallurgical science toward the center of phase diagrams, rather than relying solely on traditional alloying methods built around a single primary element. Based on the ΔS_{conf}, it is possible to subdivide these materials and alloys into three distinct groups: conventional alloys, such as steels, are presented as low-entropy alloys ($\Delta S_{conf} < 1R$); superalloys reported as medium-entropy alloys ($1R < \Delta S_{conf} < 1.5R$); and, finally, the HEA ($\Delta S_{conf} > 1.5R$), with R being the perfect gas constant [79, 80]. Initially, research in this field has predominantly focused on the development of single-phase

Table 7 Overview of turning and additional alloy design studies

Addition	Amount	Base alloy	Type of test	ν_C [m/min]	f [mm]	a_p [mm]	Evaluated criteria	Reference
Graphite + Ti	Graphite: 0–1.9 wt.% Ti: 0.5; 1 wt.%	CuZn40	Turning	~ 11.8	0.1	0.5	Cutting Forces Chip Classification	[55]
Fe_3C	5 wt.% of eutectic cast iron	CuZn40	Turning	35	0.1	0.5	Chip Classification Surface Morphology analysis	[58]
Si	Up to 1.7 wt.%	CuZn40	-	-	-	-	-	[59]
	1 wt.%	Cu62.5Si1P0.07PbZn	Turning	40	0.11	1	Cutting Forces Chip Classification	[60]
	3 wt.%	Cu75.5Si3Zn	Turning	40	0.11	1	Chip Classification	[61]
	3 wt.%	Cu76Si3PZn	Turning	400	0.05–0.3	0.5–2.5	Cutting Forces Chip Classification Tool Wear Surface Integrity Energy Consumption	[62]
	Up to 4 wt.%	CuZn40	Turning	22.6—104	0.08–0.2	0.5–1	Cutting Forces Chip Classification Tool Wear Surface Roughness—Ra	[63]
B_4C	Up to 12 wt.%	CuSi4Zn14	-	-	-	-	-	[64]
Ti_3AlC_2	Up to 5 wt.%	CuZn40	-	-	-	-	-	[65]
Si + MoS_2	Si: 0.5–1.7 wt.% Mo: 0.2–0.4 wt.% S: 0.15–0.63 wt.%	Cu63Sn3Zn	Turning	50	0.2	1	Chip Classification Surface Roughness—Ra	[66]
Sn	Up to 17.4 wt.%	CuZn30	Turning	33.4–94	0.11	0.5	Cutting Forces Chip Classification Surface Roughness—Ra	[67]
Sn + Bi	Si and Bi up to 2 wt.%	CuSi0.5Zn38	Turning	50	0.1–0.4	0.4–0.8	Cutting Forces Chip Classification	[68]
Ti	1 wt.%	CuZn40	-	-	-	-	-	[70]
Ti + Sn	Ti: 1 wt.% Sn: 0.6 wt.%	CuZn40	-	-	-	-	-	[71]
Ni + Si	Ni: 1.5 and 3 wt.% Si: 0.3 and 0.6 wt.%	CuZn20	-	-	-	-	-	[72]
Fe + Al	Fe: 0.6 wt.% Al: up to 0.7 wt.%	CuPb1Zn39	-	-	-	-	-	[73]
Mg	Up to 1.79 wt.%	CuZn35	Turning	33.4—94	0.11	0.5	Cutting Forces Chip Classification	[74]
Sb	Up to 2.34 wt.%							
Al	1.89 wt.%	CuZn35	Turning	33.4—94	0.11	1	Cutting Forces Chip Classification	[75]

alloys. This focus was primarily driven by the implementation of semi-empirical criteria based on the Hume-Rothery rules, which enabled a more precise prediction of solid solutions [81]. This emphasis was justified by the purported core effects, such as the entropy effect, lattice distortion effect, sluggish diffusion, and the cocktail effect, which were believed to distinguish HEAs from conventional alloys [81, 82]. However, due to the lack of evidence that these characteristics are exclusive to single-phase structures, there has been a significant surge in interest in the development of multiphase alloys. This shift has been driven by the implementation of strengthening concepts, such as precipitation strengthening. The concept of Complex Concentrated Alloys or Compositionally Complex Alloys (CCAs) emerged from this change in alloy development strategies. Despite this progress, numerous challenges related to the design, development, and industrialization of such alloys remain to be overcome [83, 84]. Unlike conventional alloys, the

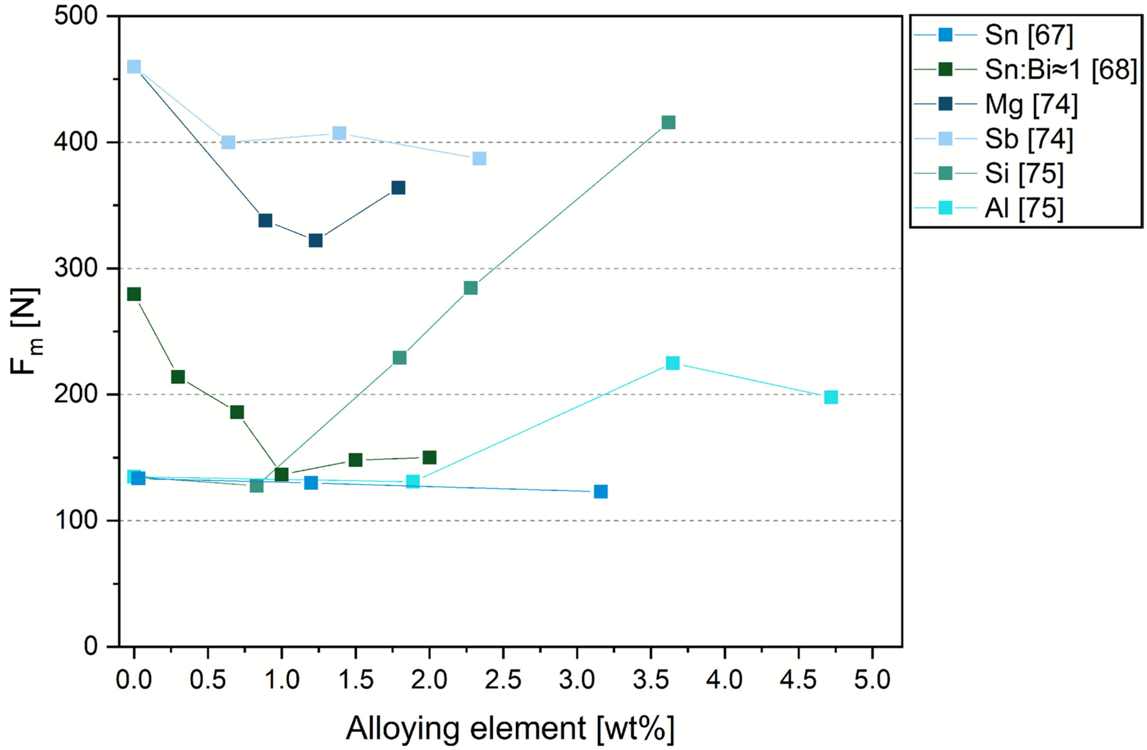

Fig. 8 Effect of alloying elements on the resultant cutting force (F_m)

most formidable challenge in HEA/CCA development is the identification and selection of alloys from the vast array of possible combinations, which depend on the type, number, and content of each element. Several approaches can facilitate alloy design and development, such as ab initio Density Functional Theory (DFT) calculations [85–87]. However, the CALculation of PHAse Diagrams (CALPHAD) methodology is considered the most practical technique for predicting and developing these alloys [88].

Currently, few researchers have employed the HEA and CCA concepts for the development of new brass alloys. For example, Laws et al. [89] were the first to introduce the concept of high-entropy brass alloys (HEBAs), in which several as-cast and heat-treated alloys based on the $[CuMnNi]_aAl_bZn_cSn_d$ $(60 < a < 80;\ 20 < b + c + d < 40)$ were studied. The alloy based on the system $[CuMnNi]_aZn_c$ showed the lowest hardness, ranging from 100 to 250 HV, and lower σ_{YS}, ranging from 140 to 215 MPa, while associated with an extremely high ductility (~60%). These observations were mainly justified by the single FCC structure or, in some cases, by the low amount of a BCC phase, which can be associated with the α and β' phases of conventional brass alloys. However, with the addition of Al and Sn, it was observed that an overall mechanical performance increase of the alloys was observed, which can be associated with the superior solid solution strengthening and with the formation of $[Cu,Mn,Ni]_3[Al,Sn]$ intermetallic structures, increasing the hardness to values around 300–350 HV.

Later, Nagase et al. [90] employed thermodynamic alloy design parameters based on the Hume-Rothery rules to develop HEBAs based on the $Cu_xZnMnNi$ (x = 1, 2, 3, 4), $Cu_2ZnMnNiSn_y$, and $CuZnMnNiSn_z$. Following such alloy design, $Cu_xZnMnNi$ (x = 1, 2, 3, 4), $CuZnMnNiSn_{0.2}$, and $Cu_2ZnMnNiSn_{0.45}$ were produced through metallic mold casting. These new alloys presented higher hardness, ranging from 180–400 HV, associated with σ_{YS} higher than 300 MPa. Regarding microstructural evolution, the authors developed an alloy map of constituent phases in the studied alloys, which aids in understanding the depicted alloys. On this same topic, Chen et al. [91] showed the possibility of resorting to CALPHAD simulation to aid with the alloy design. To prove such a concept, the same compositions of the study mentioned above were simulated through a Scheil with Back Diffusion model, showcasing that most of the results were consistent with the experimental results (except for one alloy), since all ternary partial systems in the Cu–Zn-Mn-Ni–Sn quinary system were not assessed in the database used. Additionally, Lv et al. [92] studied the corrosion behavior of these HEBAs and showed that these alloys present similar corrosion mechanisms and oxide corrosion structures that were already depicted for the dezincification of conventional brass alloys.

Chaskis et al. [93] have explored the alloy $Cu_{50}Al_{20}Zn_{25}Sn_5$, employing CALPHAD methodology, to predict phase formation and optimize the multiphase microstructure required for enhanced machinability. A multiphase alloy containing a major Cu-rich (α') matrix reinforced with a secondary Zn-rich (β') phase and pure Sn (γ') was developed (Fig. 8). The last microstructural feature can be expected to replicate the Pb effect during machining operations, as it presents high Sn content (> 85 at.%) with a considerably low melting point (~ 230 ºC). Preliminary findings, in terms of mechanical performance, show that the developed alloy presented a hardness of 532 HV 0.2, which is considerably beyond the maximum hardness observed in the current brass solution in the market. This higher hardness may represent drawbacks in further alloy processing or application; however, no machinability or dezincification tests have been conducted, so further alloy evaluation is still necessary. CALPHAD approaches have already been adopted for different sectors, and it is important to highlight the possibility of expanding such an approach to achieve a high-throughput screening of compositions, allowing for a more informed alloy composition selection [94].

Despite not explicitly mentioning the HEBAs concept, several studies have developed alloys that could fall in this category due to their high Cu and Zn content. These studies have identified several additional elements (Fig. 9), such as Co [95, 96], Si [97], Cr [98], Fe [99], Ti [100], and Pb [101, 102] as potential alloying elements. This versatility opens a significant opportunity for developing novel lead-free brass alloys within the Cu–Zn system (Fig. 10).

This approach leverages the idea that a finely tuned multiphase structure, reinforced with secondary precipitates or insoluble particles, cannot only match but potentially surpass the chip breaking capabilities of traditional leaded alloys through the incorporation of high-alloyed brass alloys. However, most of these studies do not indicate specific applications, suggesting that if well-defined target properties are established for an application-driven design approach, novel and capable DZR and FCB could be obtained.

Conclusion and Future Directions

The pursuit of machinable and high-performing lead-free brass alloys reflects a concerted effort by both scientific and industrial fields to address critical environmental, health, and performance challenges linked to conventional leaded brasses. Pb incorporation must be discontinued due to the heavy restrictions being implemented, creating a need for novel solutions that are both compliant with the new regulations and attractive to industrialization. Through this systematic review, it was possible to identify three complementary fronts where recent efforts have been focused on the following: (1) machining operations optimization through the assessment of chip breaking mechanisms, chip morphology, cutting forces, etc.; (2) heat treatments for microstructure tailoring, mainly for manipulation of α:β' ratio; and (3) on the material side, several approaches on alloying, reinforcement, and high/medium-entropy alloy design;

Alloy design strategies that incorporate reinforcements present a potentially attractive route for enhancing machinability. However, their industrial application remains limited due to high costs, processing complexities, and generally poor interfacial bonding with the matrix. In contrast, Pb substitution and entropy-based approaches have emerged as promising alternatives for developing novel, sustainable, and machinable lead-free brasses. Nevertheless, further research is required to comprehensively assess their machinability and facilitate their adoption in industrial applications. To promote a more sustainable and cost-effective alloy development, researchers could focus on low-melting-point (e.g., Al and Sn) and low-cost elements. The incorporation of such elements might lead to the formation of low-melting-point precipitates that replicate Pb-precipitates' role during machining operations, while simultaneously decreasing the alloy's melting point. This also contributes to a reduction in energy consumption in several steps of parts production, including melting, casting, and machining.

Additionally, both heat treatments and machining parameter optimization should be considered for a further tailoring of both microstructural, mechanical and machining characteristics, allowing for an application-driven design.

Finally, based on the present systematic review, some guidelines can be highlighted to lay the path for future research in the field of lead-free brass alloys:

1. Due to the synergistic effect of multi-alloying addition, novel alloy design approaches must be implemented, such as ab initio calculations and CALPHAD simulations, for a better understanding of the role of each element in phase transformation, mechanical performance, etc. This could lead to a new path of high-throughput composition screening, personalized alloy definition, and thermo-mechanical processing optimization, aiming for application-driven design established on both experimental and thermodynamic data.
2. This review highlights a lack of standardized methodologies in machining assessments. To enhance comparability between conventional and novel alloys, the authors recommend adopting experimental designs that align with machining parameters commonly reported in the literature. This could integrate the evaluation of cutting forces through turning tests with a v_c of 50 m/min, f of 0.1 mm (per rev), and an a_p between 0.5 to 1 mm, allowing for a full machinability assessment (cutting forces,

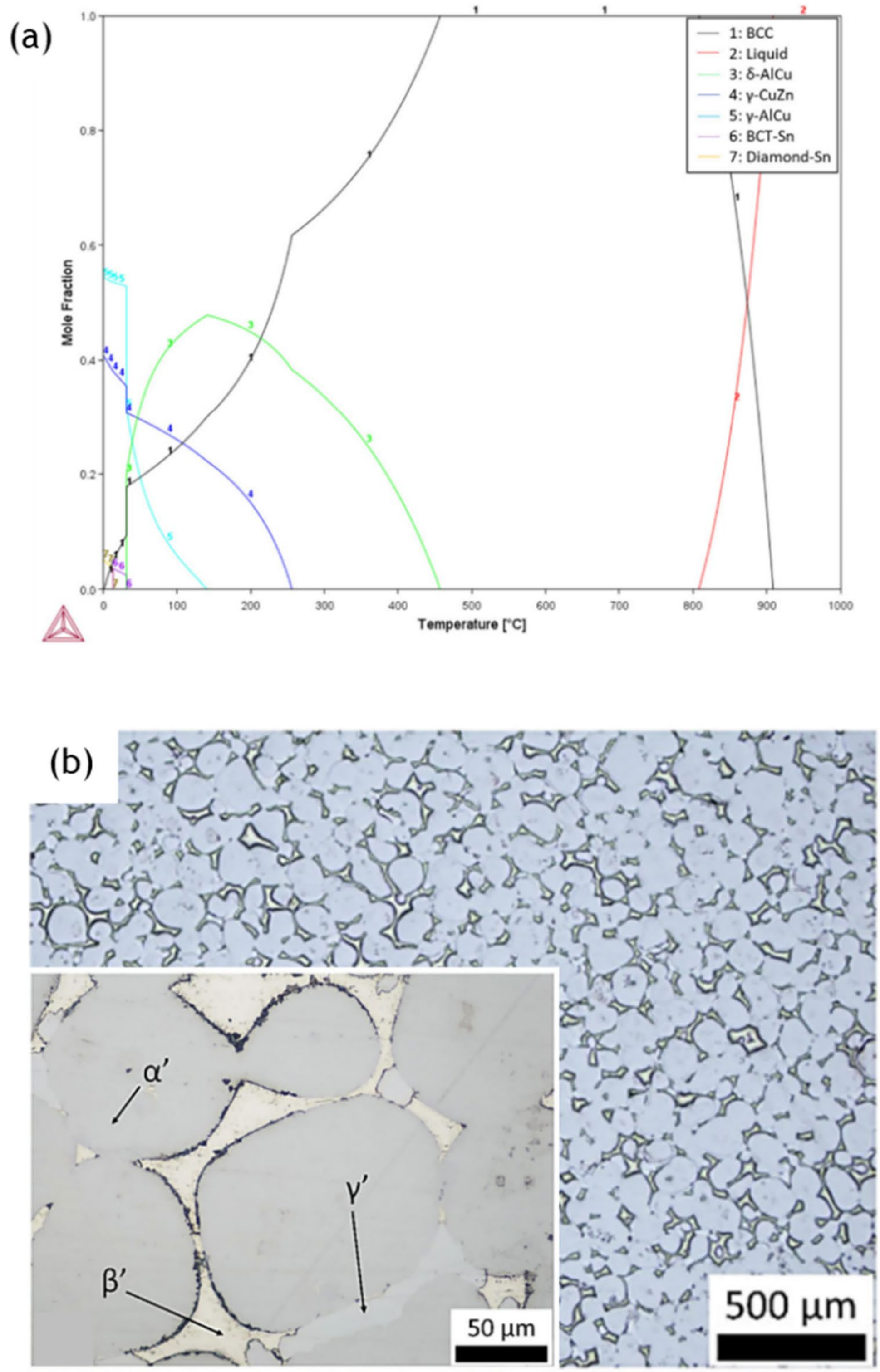

Fig. 9 **a** Calculated mole fraction diagram of the Cu50Zn25Al20Sn5 at. % system with Thermo-Calc Software and **b** alloy homogenized for 16 h at 550 ºC, followed by furnace cooling. Adapted from [92]

chips formation and machinability index based on the resultant cutting force).

3. Design of experiments, ANOVA, Taguchi method, and additional advanced statistical tools should be considered for a complex understanding of the multi-interactions between machining parameters and machinability characteristics of brass alloys. By considering both compositions, thermo-mechanical processing, machin-

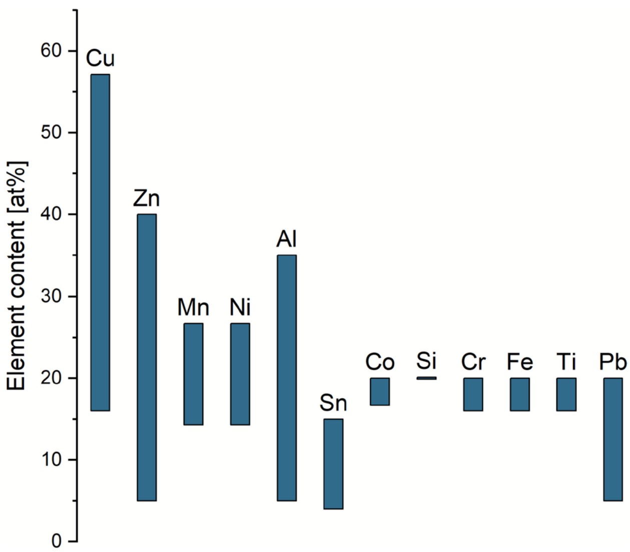

Fig. 10 Elements and respective quantities considered in HEBAs or HEAs similar systems [89–102]

ing parameters and respective outputs (microstructure, mechanical properties and machinability variables), it is possible to define a robust optimization approach that saves both money and time in the industrial environment. This is achieved by the construction of in-house databases to provide accurate data to such statistical models.

Authors Contributions Conceptualization, B.L.R. and E.W.S.; formal analysis, B.L.R., J.M., and M.T.; funding acquisition, M.B. and E.W.S.; project administration, E.W.S.; supervision, M.B. and E.W.S.; writing – original draft, B.L.R., J.M., M.T.; writing – review and editing, R.F.S., M.B., and E.W.S. All authors have read and agreed to the published version of the manuscript.

Funding This research was supported by Project "recyBRASS" - COMPETE2030-FEDER-00576900 – funded by FEDER and FSE+ funds through the COMPETE 2030 Program. Bernardo L. Ribeiro received funding for scientific research through a PhD studentship from the Portuguese Foundation for Science and Technology (FCT) under the reference 2024.01517.BDANA. The authors acknowledge the Portuguese Foundation for Science and Technology (FCT) for its financial support to LAETA via the project UID/50022/2025 (DOI: https://doi.org/10.54499/UID/50022/2025).

Declarations

Conflicts of interest The authors declare no conflicts of interest.

References

1. Gupta K, Jain NK, Laubscher R (2017) Introduction to gear engineering. Advanced gear manufacturing and finishing. Elsevier, Amsterdam, pp 1–33
2. Davis JR (2001) Wrought copper and copper alloys. ASM special handbook—copper and copper alloys, 5th edn. ASM International, Detroit, pp 54–84
3. Konečná R, Fintová S (2012) Copper alloys—early applications and current performance—enhancing processes. IntechOpen. https://doi.org/10.5772/1912
4. Goswami R, Chattopadhyay K, Ryder PL (1998) Melting of Pb particles embedded in Cu-Zn matrices. Acta Mater 46(12):4257–4271. https://doi.org/10.1016/S13596454(98)000949--
5. Gane N (1981) The effect of lead on the friction and machining of brass. Philos Mag A 43(3):545–566. https://doi.org/10.1080/01418618108240394
6. Stoddart CTH, Lea C, Dench WA, Green P, Pettit HR (1979) Relationship between lead content of Cu-40Zn, machinability, and svvarf surface composition determined by Auger electron spectroscopy. Metals Technol 6(1):176–184. https://doi.org/10.1179/030716979803276435
7. Johansson J, Alm P, M'Saoubi R, Malmberg P, Ståhl J-E, Bushlya V (2022) On the function of lead (Pb) in machining brass alloys. Int J Adv Manuf Technol 120(11–12):7263–7275. https://doi.org/10.1007/s00170-022-09205-0
8. Hofmann U, El-Magd E (2005) Behaviour of Cu-Zn alloys in high speed shear tests and in chip formation processes. Mater Sci Eng A 395(1–2):129–140. https://doi.org/10.1016/j.msea.2004.12.030
9. Laakso SVA, Johansson J, Johansson D, Schultheiss F, Ståhl J-E (2019) Multi-objective testing of different brass alloy components for DFM. Procedia CIRP 81:127–132. https://doi.org/10.1016/j.procir.2019.03.023
10. Bjerke A et al (2021) Thermodynamic modeling framework for prediction of tool wear and tool protection phenomena in machining. Wear 484–485:203991. https://doi.org/10.1016/j.wear.2021.203991
11. Copper Development Association Inc. (2000) Introduction to brasses. https://www.copper.org/publications/newsletters/innovations/2000/01/brasses.html. Accessed 26 May 2025
12. Maher BA, Moore C, Matzka J (2008) Spatial variation in vehicle-derived metal pollution identified by magnetic and elemental analysis of roadside tree leaves. Atmos Environ 42(2):364–373. https://doi.org/10.1016/j.atmosenv.2007.09.013
13. Fertmann R, Hentschel S, Dengler D, Janßen U, Lommel A (2004) Lead exposure by drinking water: an epidemiologial study in Hamburg, Germany. Int J Hyg Environ Health 207(3):235–244. https://doi.org/10.1078/1438-4639-00285
14. International Labour Organization (2023) Exposure to lead in the world of work, Geneva. https://www.ilo.org/sites/default/files/wcmsp5/groups/public/%40ed_dialogue/%40lab_admin/documents/publication/wcms_894143.pdf. Accessed 26 May 2025

15. Zhu T, Li W, Kwok JCM, Siu KW, Yin L, Ngan AHW (2023) Metallurgical pathways of lead leaching from brass. NPJ Mater Degrad. https://doi.org/10.1038/s41529-023-00389-8
16. European Parliament (2022) Directive (EU) 2020/2184 of the European Parliament and of the Council of 16 December 2020 on the quality of water intended for human consumption. Official Journal of the European Union
17. 4 MS Common Approach (2020) Acceptance of metallic materials used for products in contact with drinking water Procedure for the acceptance of metallic materials for PDW
18. European Union (2006) Regulation (EC) No 1907/2006 - Registration, Evaluation, Authorisation and Restriction of Chemicals (REACH) Latest update: 27/04/2021. https://osha.europa.eu/pt/legislation/directives/regulation-ec-no-1907-2006-of-the-european-parliament-and-of-the-council. Accessed 14 Feb 2024
19. European Union (2000) Directive 2000/53/EC of the European Parliament and of the Council of 18 September 2000 on end-of life vehicles. https://eur-lex.europa.eu/legal-content/EN/TXT/?uri=CELEX%3A02000L0053-20230330. Accessed 14 Feb 2024
20. European Union (2011) Directive 2011/65/EU of the European Parliament and of the Council of 8 June 2011 on the restriction of the use of certain hazardous substances in electrical and electronic equipment. https://eur-lex.europa.eu/legal-content/EN/TXT/?uri=CELEX:02011L0065-20160715. Accessed 14 Feb 2024
21. Copper Development Association Inc. The economic value of brass recycling and high-speed machining. https://highspeedmachiningbrass.com/wp-content/uploads/2020/08/Recycling-Brass-WhitePaper.pdf#:~:text=The%20inherent%20material%20properties%20of%20brass%20remain,the%20purchase%20price%20of%20the%20raw%20material. Accessed 24 Mar 2025
22. Copper Development Association Inc. Brass rod: a poster child for sustainability. https://www.copper.org/choosebrass/pdf/brass-rod-a-poster-child-for-sustainability.php#:~:text=Brass%20is%20one%20of%20the,keeps%20waste%20out%20of%20landfills. Accessed 24 Mar 2025
23. Copper Development Association Inc. (2020) The circular economy of brass recycling. https://highspeedmachiningbrass.com/the-circular-economy-of-brass-recycling/. Accessed 14 Feb 2024
24. Estelle AA (2016) Drinking water lead regulations: impact on the brass value chain. Mater Sci Technol 32(17):1763–1770. https://doi.org/10.1080/02670836.2016.1220906
25. Loibl A, Tercero Espinoza LA (2021) Current challenges in copper recycling: aligning insights from material flow analysis with technological research developments and industry issues in Europe and North America. Resour Conserv Recycl 169. https://doi.org/10.1016/j.resconrec.2021.105462
26. Page MJ et al (2021) The PRISMA 2020 statement: an updated guideline for reporting systematic reviews. BMJ. https://doi.org/10.1136/bmj.n71
27. Kohl C et al (2018) Online tools supporting the conduct and reporting of systematic reviews and systematic maps: a case study on CADIMA and review of existing tools. Environ Evid 7(1):8. https://doi.org/10.1186/s13750-018-0115-5
28. Kuyucak S, Sahoo M (1996) A review of the machinability of copper—base alloys. Can Metall Q 35(1):1–15. https://doi.org/10.1179/cmq.1996.35.1.1
29. Tang Y, Ma J, Han D, Wang J, Qi H, Jin L (2022) Critical evaluation and thermodynamic optimization of the Cu-Zn, Cu-Se and Zn-Se binary systems. Metals 12(9):1401. https://doi.org/10.3390/met12091401
30. Collini L (2012) Copper alloys—early applications and current performance—enhancing processes. InTech. https://doi.org/10.5772/1912
31. University of Cambridge, Micrograph Library—Cu-Zn. https://www.doitpoms.ac.uk/miclib/compositions.php?id=13. Accessed 01 Feb 2024
32. Das K, Bandyopadhyay TK (2001) Application of differential scanning calorimetry (DSC) kinetic methods to determine the kinetic parameters of α precipitation in a 60/40 brass. Scr Mater 44(11):2597–2603. https://doi.org/10.1016/S1359-6462(01)00921-6
33. Thermo-Calc. TCCU6 technical information. https://thermocalc.com/wp-content/uploads/Documentation/Databases/Thermodynamic/tccu6-technical-info.pdf. Accessed 01 Feb 2024
34. International Organization for Standardization (2025) ISO 6509–1:2014 Corrosion of metals and alloys—Determination of dezincification resistance of copper alloys with zinc. Part 1: Test method, 2014, International Organization for Standardization, Geneva, Switzerland. https://www.iso.org/standard/54666.html. Accessed 19 May 2025
35. Kundig KJA (2025) Free-cutting brass: a closed environmental loop. Copper Development Association. https://copper.org/publications/newsletters/innovations/1998/07/brass360.php. Accessed 19 May 2025
36. Liao Z et al (2024) Review of current best-practices in machinability evaluation and understanding for improving machining performance. CIRP J Manuf Sci Technol 50:151–184. https://doi.org/10.1016/j.cirpj.2024.02.008
37. Syreyshchikova NV et al (2020) A study on the machinability of steels and alloys to develop recommendations for setting tool performance characteristics and belt grinding modes. Materials 13(18):3978. https://doi.org/10.3390/ma13183978
38. Mitsubishi Materials, GloBrass and ECO BRASS — Lead-free brass with excellent machinability. https://www.mitsubishi-copper.com/en/products/materials/ecobrass/. Accessed 30 Dec 2023
39. Johansson J (2022) Towards sustainable manufacturing of brass components charaterisation. Lund University, Machinability and Solid-State Recycling of Lead-Free Brass
40. Kupferverband (2024) Richtwerte für die spanende Bearbeitung von Kupfer und Kupferlegierungen. www.kupfer.de
41. Brans K, Baier S, Schraknepper D, Bergs T (2022) Empirical studies on the influence of tool and process parameters on the machinability in plunge milling of lead—free CuZn-alloys. Procedia CIRP 115:113–118. https://doi.org/10.1016/j.procir.2022.10.059
42. Müller MS, Sørby K (2024) Investigations on chip breakability in lead-free brass alloy CW511L using different chip breaking geometries. Procedia CIRP 126:453–457. https://doi.org/10.1016/j.procir.2024.08.399
43. Nobel C, Hofmann U, Klocke F, Veselovac D (2015) Experimental investigation of chip formation, flow, and breakage in free orthogonal cutting of copper-zinc alloys. Int J Adv Manufact Technol. https://doi.org/10.1007/s00170-015-7749-z
44. Tascioglu E, Zoghipour N, Sharif S, Kaynak Y (2022) Machining-induced surface integrity in brass alloys. Procedia CIRP 108:654–659. https://doi.org/10.1016/j.procir.2022.04.078
45. Das A, Bajpai V (2023) Machinability analysis of lead free brass in high speed micro turning using minimum quantity lubrication. CIRP J Manuf Sci Technol 41:180–195. https://doi.org/10.1016/j.cirpj.2022.11.023
46. Toulfatzis A, Pantazopoulos G, David C, Sagris D, Paipetis A (2018) Machinability of eco-friendly lead-free brass alloys: Cutting—force and surface—roughness optimization. Metals 8(4):250. https://doi.org/10.3390/met8040250
47. Toulfatzis AI, Pantazopoulos GA, Paipetis AS (2016) Microstructure and properties of lead-free brasses using post-processing

heat treatment cycles. Mater Sci Technol 32(17):1771–1781. https://doi.org/10.1080/02670836.2016.1221493
48. Moriarty M, Wu Y, Murray T, Hutchinson C (2021) The effect of phase fraction, size and shape on the dezincification of duplex brasses. Corros Sci 184:109366. https://doi.org/10.1016/j.corsci.2021.109366
49. Toulfatzis AI, Pantazopoulos GA, David CN, Sagris DS, Paipetis AS (2018) Final heat treatment as a possible solution for the improvement of machinability of Pb-free brass alloys. Metals 8(8):575. https://doi.org/10.3390/met8080575
50. Brans K, Kind S, Meurer M, Bergs T (2024) Influence of the material production route on the material properties and the machinability of the lead-free copper-zinc-alloy CuZn40 (CW509L). Metals 14(7):747. https://doi.org/10.3390/met14070747
51. Sathishkumar N et al (2024) Impact of heat treatment process on machinability behavior of brass alloy 272(CuZn37). Mater Today Proc. https://doi.org/10.1016/j.matpr.2024.02.025
52. Basori I, Gadhu R, Sofyan BT (2017) Effects of deformation and annealing temperature on the microstructures and hardness of Cu-29Zn-0.6Bi brass. Key Eng Mater 748:218–223. https://doi.org/10.4028/www.scientific.net/KEM.748.218
53. Babouri L, Belmokre K, Kabir A, Abdelouas A, Khettabi R, El Mendili Y (2019) Microstructure and crystallographic properties of $Cu_{77}Zn_{21}$ alloy under the effect of heat treatment. Mater High Temp 36(2):165–172. https://doi.org/10.1080/09603409.2018.1499243
54. Imai H et al (2010) Characteristics and machinability of lead-free P/M Cu60–Zn40 brass alloys dispersed with graphite. Powder Technol 198(3):417–421. https://doi.org/10.1016/j.powtec.2009.12.010
55. Zhang X, Ma C, Li S, Pan D, Zheng F (2020) Interface design of lead-free free-cutting titanium reinforced graphite brass composites and its effect on mechanical properties and cutting performance. Mater Sci Eng A 774:138909. https://doi.org/10.1016/j.msea.2020.138909
56. Imai H, Shufeng L, Atsumi H, Kosaka Y, Kojima A, Kondoh K (2010) Development of lead-free machinable brass with bismuth and graphite particles by powder metallurgy process. Mater Trans 51(5):855–859. https://doi.org/10.2320/matertrans.MH200907
57. Li S, Imai H, Umeda J, Fu Y, Kondoh K (2016) Investigation of high-strength lead-free machinable Cu40Zn duplex graphite brasses by powder metallurgy. Mater Sci Technol 32(17):1751–1756. https://doi.org/10.1080/02670836.2016.1246098
58. Zhuo H, Tang J, Xue Y, Ye N (2015) Preparation of lead-free free-cutting graphite brasses by graphitization of cementite. Trans Nonferrous Met Soc China 25(10):3252–3257. https://doi.org/10.1016/S1003-6326(15)63961-9
59. Doostmohammadi H, Moridshahi H (2015) Effects of Si on the microstructure, ordering transformation and properties of the Cu60Zn40 alloy. J Alloys Compd 640:401–407. https://doi.org/10.1016/j.jallcom.2015.03.228
60. Oishi K, Goto H, Suzaki K, Oka T, Mori H (2023) Development of next-generation lead-free free-cutting α + β brass. Mater Trans. https://doi.org/10.2320/matertrans.MT-D2022006
61. Suzaki K, Goto H, Tabuchi T, Mori H, Oishi K (2023) Study on machinability of lead-free α + β brass 62.5Cu–1Si–Zn alloy. Mater Trans. https://doi.org/10.2320/matertrans.MT-D2022007
62. Schultheiss F, Windmark C, Sjöstrand S, Rasmusson M, Ståhl J-E (2018) Machinability and manufacturing cost in low-lead brass. Int J Adv Manuf Technol 99(9–12):2101–2110. https://doi.org/10.1007/s00170-018-1866-4
63. Taha MA, El-Mahallawy NA, Hammouda RM, Moussa TM, Gheith MH (2012) Machinability characteristics of lead free-silicon brass alloys as correlated with microstructure and mechanical properties. Ain Shams Eng J 3(4):383–392. https://doi.org/10.1016/j.asej.2012.05.004
64. Clinktan R, Ramkumar KR, Sivasankaran S (2020) Effect of boron carbide addition on strengthening mechanisms, cold workability and instantaneous strain hardening behaviour of Cu4Si14Zn nanocomposites. Mater Sci Eng A 787:139538. https://doi.org/10.1016/j.msea.2020.139538
65. Peng F et al (2024) Microstructure, mechanical and tribological properties of Cu40Zn-Ti3AlC2 composites by powder metallurgy. Lubricants 12(9):306. https://doi.org/10.3390/lubricants12090306
66. Semih Ö, Recep A (2023) Investigation of microstructure, machinability, and mechanical properties of new-generation hybrid lead-free brass alloys. High Temp Mater Processes. https://doi.org/10.1515/htmp-2022-0263
67. Rajabi Z, Doostmohammadi H (2018) Effect of addition of tin on the microstructure and machinability of α - brass. Mater Sci Technol 34(10):1218–1227. https://doi.org/10.1080/02670836.2018.1435484
68. Suksongkarm P, Rojananan S, Rojananan S (2017) Using recycled bismuth-tin solder in novel machinable lead-free brass. Mater Trans 58(12):1754–1760. https://doi.org/10.2320/matertrans.M2017227
69. Atsumi H, Imai H, Li S, Kondoh K, Kousaka Y, Kojima A (2011) High-strength, lead-free machinable α–β duplex phase brass Cu–40Zn–Cr–Fe–Sn–Bi alloys. Mater Sci Eng A 529:275–281. https://doi.org/10.1016/j.msea.2011.09.029
70. Li S, Imai H, Atsumi H, Kondoh K (2011) Contribution of Ti addition to characteristics of extruded Cu40Zn brass alloy prepared by powder metallurgy. Mater Des 32(1):192–197. https://doi.org/10.1016/j.matdes.2010.06.008
71. Li S et al (2012) Development of precipitation strengthened brass with Ti and Sn alloying elements additives by using water atomized powder via powder metallurgy route. Mater Chem Phys 135(2–3):644–652. https://doi.org/10.1016/j.matchemphys.2012.05.039
72. Chen W et al (2022) Effect of Ni2Si precipitates on microstructure and mechanical properties of Cu–Zn brasses. Metals Mater Int 28(10):2555–2562. https://doi.org/10.1007/s12540-021-01153-w
73. Li X, Ma B, Wang C, Chen Y (2024) Microstructure evolution and properties improvement of Fe-containing scrap brass alloy by Al microalloying and dispersion distribution regulation. Int J Metalcast 18(4):2907–2923. https://doi.org/10.1007/s40962-023-01213-4
74. Adineh M, Doostmohammadi H, Raiszadeh R (2019) Effect of Si and Al on the microstructure, mechanical properties and machinability of 65Cu-35Zn brass. Iran J Mater Sci Eng. https://doi.org/10.22068/ijmse.16.2.21
75. Adineh M, Doostmohammadi H (2019) Microstructure, mechanical properties and machinability of Cu-Zn-Mg and Cu-Zn-Sb brass alloys. Mater Sci Technol 35(12):1504–1514. https://doi.org/10.1080/02670836.2019.1630089
76. German Copper Institute (2010) Recommended machining parameters for copper and copper alloys
77. Cantor B, Chang ITH, Knight P, Vincent AJB (2004) Microstructural development in equiatomic multicomponent alloys. Mater Sci Eng A 375:213–218. https://doi.org/10.1016/j.msea.2003.10.257
78. Yeh J-W et al (2004) Nanostructured high-entropy alloys with multiple principal elements: novel alloy design concepts and outcomes. Adv Eng Mater 6(5):299–303. https://doi.org/10.1002/adem.200300567
79. Otto F, Yang Y, Bei H, George EP (2013) Relative effects of enthalpy and entropy on the phase stability of equiatomic

high-entropy alloys. Acta Mater 61(7):2628–2638. https://doi.org/10.1016/j.actamat.2013.01.042
80. Murty BS, Yeh JW, Ranganathan S (2014) High-entropy alloys. High entropy alloys. Elsevier, Amsterdam, pp 13–35
81. Senkov ON, Miracle DB, Chaput KJ, Couzinie J-P (2018) Development and exploration of refractory high entropy alloys—a review. J Mater Res 33(19):3092–3128. https://doi.org/10.1557/jmr.2018.153
82. Anamu US et al (2023) Fundamental design strategies for advancing the development of high entropy alloys for thermo-mechanical application: a critical review. J Mater Res Technol 27:4833–4860. https://doi.org/10.1016/j.jmrt.2023.11.008
83. Mukherjee S (2020) Complex Concentrated Alloys (CCAs)—current understanding and future opportunities. Metals 10(9):1253. https://doi.org/10.3390/met10091253
84. Beyerlein IJ, Cao P, Pollock TM (2023) Complex concentrated alloys and chemical short-range ordering. MRS Bull 48(7):746–752. https://doi.org/10.1557/s43577-023-00567-8
85. Karabin M et al (2022) Ab initio approaches to high-entropy alloys: a comparison of CPA, SQS, and supercell methods. J Mater Sci 57(23):10677–10690. https://doi.org/10.1007/s10853-022-07186-9
86. Yuan G, Wu M, Ruiz Pestana L (2023) Density functional theory-machine learning characterization of the adsorption energy of oxygen intermediates on high-entropy alloys made of earth-abundant metals. J Phys Chem C 127(32):15809–15818. https://doi.org/10.1021/acs.jpcc.3c03404
87. Clausen CM, Nielsen MLS, Pedersen JK, Rossmeisl J (2023) Ab initio to activity: machine learning-assisted optimization of high-entropy alloy catalytic activity. High Entropy Alloys Mater 1(1):120–133. https://doi.org/10.1007/s44210-022-00006-4
88. van de Walle A, Sun R, Hong Q-J, Kadkhodaei S (2017) Software tools for high-throughput CALPHAD from first-principles data. Calphad 58:70–81. https://doi.org/10.1016/j.calphad.2017.05.005
89. Laws KJ et al (2015) High entropy brasses and bronzes—microstructure, phase evolution and properties. J Alloys Compd 650:949–961. https://doi.org/10.1016/j.jallcom.2015.07.285
90. Nagase T, Shibata A, Matsumuro M, Takemura M, Semboshi S (2019) Alloy design and fabrication of ingots in Cu-Zn-Mn-Ni-Sn high-entropy and Cu-Zn-Mn-Ni medium-entropy brasses. Mater Des 181:107900. https://doi.org/10.1016/j.matdes.2019.107900
91. Li Q, Chan YC, Zhang K, Yung KC (2014) Study of microstructure evolution in novel Sn–Zn/Cu bi-layer and Cu/Sn–Zn/Cu sandwich structures with nanoscale thickness for 3D packaging interconnection. Microelectron Eng 122:52–58. https://doi.org/10.1016/j.mee.2014.03.002
92. Lv Y, Lang X, Zhang Q, Liu W, Liu Y (2022) Study on corrosion behavior of (CuZnMnNi)100−xSnx high-entropy brass alloy in 5 wt% NaCl solution. J Alloys Compd 921:166051. https://doi.org/10.1016/j.jallcom.2022.166051
93. Chaskis S, Maritsa S, Stavroulakis P, Papadopoulou S, Goodall R, Papaefthymiou S (2024) Compositional design and thermal processing of a novel lead-free Cu–Zn–Al–Sn medium entropy brass alloy. Metals (Basel) 14(6):620. https://doi.org/10.3390/met14060620
94. Feng R et al (2021) High-throughput design of high-performance lightweight high-entropy alloys. Nat Commun 12(1):4329. https://doi.org/10.1038/s41467-021-24523-9
95. Salemi F, Abbasi MH, Karimzadeh F (2016) Synthesis and thermodynamic analysis of nanostructured CuNiCoZnAl high entropy alloy produced by mechanical alloying. J Alloys Compd 685:278–286. https://doi.org/10.1016/j.jallcom.2016.05.274
96. Mohanty S, Gurao NP, Padaikathan P, Biswas K (2017) Ageing behaviour of equiatomic consolidated Al 20 Co 20 Cu 20 Ni 20 Zn 20 high entropy alloy. Mater Charact 129:127–134. https://doi.org/10.1016/j.matchar.2017.04.011
97. Sharma A, Oh MC, Ahn B (2020) Microstructural evolution and mechanical properties of non-Cantor AlCuSiZnFe lightweight high entropy alloy processed by advanced powder metallurgy. Mater Sci Eng A 797:140066. https://doi.org/10.1016/j.msea.2020.140066
98. Mridha S, Samal S, Khan PY, Biswas K, Govind, (2013) Processing and Consolidation of Nanocrystalline Cu-Zn-Ti-Fe-Cr High-Entropy Alloys via Mechanical Alloying. Metal Mater Trans A 44(10):4532–4541. https://doi.org/10.1007/s11661-013-1824-6
99. Chae MJ, Lee H, Sharma A, Ahn B (2021) Effect of light (X = Mg, Si) and heavy (X = Zn) metals on the microstructural evolution and densification of AlCuFeMnTi-X high-entropy alloy processed by advanced powder metallurgy. Powder Metall 64(3):228–234. https://doi.org/10.1080/00325899.2021.1909212
100. Varalakshmi S, Kamaraj M, Murty BS (2010) Processing and properties of nanocrystalline CuNiCoZnAlTi high entropy alloys by mechanical alloying. Mater Sci Eng A 527(4–5):1027–1030. https://doi.org/10.1016/j.msea.2009.09.019
101. Yadav S, Kumar A, Biswas K (2018) Wear behavior of high entropy alloys containing soft dispersoids (Pb, Bi). Mater Chem Phys 210:222–232. https://doi.org/10.1016/j.matchemphys.2017.06.020
102. Yadav S, Sarkar S, Aggarwal A, Kumar A, Biswas K (2018) Wear and mechanical properties of novel (CuCrFeTiZn)100-xPbx high entropy alloy composite via mechanical alloying and spark plasma sintering. Wear 410–411:93–109. https://doi.org/10.1016/j.wear.2018.05.023